INFORMATION TO USERS

This manuscript has been reproduced from the microfilm master. UMI films the text directly from the original or copy submitted. Thus, some thesis and dissertation copies are in typewriter face, while others may be from any type of computer printer.

The quality of this reproduction is dependent upon the quality of the copy submitted. Broken or indistinct print, colored or poor quality illustrations and photographs, print bleedthrough, substandard margins, and improper alignment can adversely affect reproduction.

In the unlikely event that the author did not send UMI a complete manuscript and there are missing pages, these will be noted. Also, if unauthorized copyright material had to be removed, a note will indicate the deletion.

Oversize materials (e.g., maps, drawings, charts) are reproduced by sectioning the original, beginning at the upper left-hand corner and continuing from left to right in equal sections with small overlaps. Each original is also photographed in one exposure and is included in reduced form at the back of the book.

Photographs included in the original manuscript have been reproduced xerographically in this copy. Higher quality 6" x 9" black and white photographic prints are available for any photographs or illustrations appearing in this copy for an additional charge. Contact UMI directly to order.

UMI

A Bell & Howell Information Company
300 North Zeeb Road, Ann Arbor MI 48106-1346 USA
313/761-4700 800/521-0600

REDUCTION OF ELECTROMAGNETIC INTERFERENCE IN MULTIPLE SWITCHED MODE POWER SUPPLIES

by

Susan Mack Theodore

A Thesis Submitted to the Faculty of the

DEPARTMENT OF ELECTRICAL AND COMPUTER ENGINEERING

In Partial Fulfillment of the Requirements
For the Degree of

MASTER OF SCIENCE

In the Graduate College

THE UNIVERSITY OF ARIZONA

1995

STATEMENT BY AUTHOR

This thesis has been submitted in partial fulfillment of requirements for an advanced degree at the University of Arizona and is deposited in the University Library to be made available to borrowers under rules of the Library.

Brief quotations from this thesis are allowable without special permission, provided that accurate acknowledgment of the source is made. Requests for permission for extended quotation from or reproduction of this manuscript in whole or in part may be granted by the head of the major department or the Dean of the Graduate College when in his or her judgment the proposed use of the material is in the interests of scholarship. In all other instances, however, permission must be obtained from the author.

SIGNED: Susan M. Theodore

APPROVAL BY THESIS DIRECTOR

This thesis has been approved on the date shown below:

Arthur F Witulski — 12/19/95

Arthur F. Witulski — Date

Associate Professor of Electrical
and Computer Engineering

ACKNOWLEDGMENTS

I gratefully acknowledge the help that Dr. Art Witulski gave me during the research and writing of this work. His interest in teaching coupled with his support and encouragement made this experience a rewarding one.

I also wish to acknowledge the support and commitment that the people at Allied Signal in Tucson, Arizona gave me during the research and experimental stages of this work. Special acknowledgments go to Kim Merley and Mike Barlage whose patience and support made this work possible.

TABLE OF CONTENTS

TABLE OF CONTENTS-*Continued*

LIST OF FIGURES

LIST OF FIGURES-*Continued*

LIST OF FIGURES-*Continued*

LIST OF FIGURES-*Continued*

ABSTRACT

A method to reduce Electromagnetic Interference (EMI) of multiple switching waveforms by harmonic cancellation is presented. The waveforms considered are input currents generated by 'n' Discontinuous Mode (DCM) Flyback Switched Mode Power Supplies (SMPS) that share a common source. The waveforms are modeled as ideal triangular waveforms and a Fourier analysis is performed to determine the phase relationship, θ, that minimizes the EMI. The combined EMI is minimum when $\theta = 360°/n$ and maximum when $\theta = 0°$. A system of two DCM Flyback SMPS is designed in such a way that both 0° and 180° phase shifts between input current waveforms are possible. In both cases EMI filters are designed to meet EMI standard MIL-STD-461. The system is simulated and constructed and the experimental results are presented. These results demonstrate the accuracy of the modeled waveform and the reduction of conducted EMI when optimal phasing is achieved.

CHAPTER 1

INTRODUCTION

1.0 Outline of Work

In this work a method is developed to reduce the amount of conducted Electromagnetic Interference (EMI) generated by a system of Switched Mode Power Supplies (SMPS) with a common input source. This is accomplished by optimizing the phase relationships that exist between the input current waveforms generated by the individual SMPS.

Chapter 1 begins with a review of Discontinuous Conduction Mode (DCM) Flyback SMPS. This is followed by a brief discussion of the type of conducted EMI that results from the triangular input current waveforms generated by SMPS. The EMI limit and filtering technique that will be used in this work is also presented at this time. The last part of Chapter 1 contains a description of a typical system of multiple DCM Flyback SMPS. This system illustrates how the phase relationship between the individual SMPS input current waveforms determines the amount of EMI that is conducted onto the voltage bus.

In Chapter 2 the system of Chapter 1 is simplified to the extent that the SMPS have identical switching frequencies and the input current waveforms are modeled by ideal triangular waveforms. In this chapter, reducing the conducted EMI of this system by optimizing the phase relationship between input current waveforms generated by the individual converters is studied theoretically. Since the amount of EMI is obtained by transforming the combined input current waveform from the time domain into the frequency domain by a Fourier transform, a review of this type of transformation is also presented. It is then shown that given a system of n identical SMPS with triangular input

current waveforms, the amount of conducted EMI is minimized when the phase shift between each input current waveform is equal to 360°/n.

Since this 'ideal' system does not exist in practice, Chapter 2 also investigates the possibility of using phase shifting to reduce the amount of conducted EMI when the individual input current waveforms are not identical. The amount of conducted EMI is minimized even if there exist small variations between individual converters. This is true as long as the switching frequency is the same for each SMPS and the phase shift between the individual input current waveforms is equal to 360°/n.

Chapter 3 contains the design, simulation and experimental results of a system of two parallel DCM Flyback converters with similar switching frequencies. The input current waveforms generated by each converter are first combined on the voltage bus with a phase shift of 0° and then combined with a phase shift of 180°. The resulting EMI is measured and compared for each case. When the waveforms are combined with a phase shift of 180° the resultant EMI is found to be substantially lower than in the previous case, even though the waveforms are not identical.

Although there is a substantial reduction in the amount of EMI when the non ideal converters are combined with a phase shift of 180°, the system EMI in both cases exceeds the EMI limits discussed in Chapter 1. EMI filters are required to reduce the amount of system EMI to an acceptable level for both types of phase conditions. The second part of Chapter 3 contains the design, simulation, construction and measured results for both EMI filters. When the two input current waveforms are combined with a phase shift of 180°, the amount of EMI filtering is one fourth the amount required when the phase shift is 0°. The measured amount of EMI for both filtered outputs is found to be very close to the simulated value.

1.1 Previous Work

The use of Switched Mode Power Supplies (SMPS) has many advantages over the use of Linear Power Supplies but they are definitely at a disadvantage when it comes to the amount of EMI they generate. In fact, one of the most challenging aspects of designing and manufacturing these types of power supplies is being able to meet the Electromagnetic Interference (EMI) standards. Since the advantages of using SMPS still out-weigh the disadvantages it is not surprising that a considerable amount of research has been directed towards reducing the amount of EMI generated by SMPS. One approach uses Pulse Width Modulation techniques to more evenly distribute the EMI over frequency [1]. Another approach uses noise separators to distinguish the Common Mode noise from the Differential Mode noise thus minimizing the size of the EMI filter [2,3]. The effects that the EMI filter has on the operation and stability of the SMPS has been thoroughly investigated [4,5], and the use of a quasi-resonant instead of pulse width modulated switching scheme is also shown to reduce the amount of EMI [6].

None of these previous works investigates the effects that the phase relationship between multiple SMPS operating off of the same voltage bus has on the amount of EMI that is conducted onto that voltage bus. This work determines the optimal phase relationship that minimizes the amount of EMI that is conducted onto the voltage bus from a system of multiple SMPS. A systematic analysis containing the design, simulation and experimental results of the minimized EMI filter is also included in this work.

1.2 Review of the Discontinuous Conduction Mode Flyback Converter

There are basically three types of power supply designs: Linear, Switched Mode and Resonant Converter. The Linear power supply has an efficiency of 30-50% and is typically used in low power applications. The Switched Mode Power Supply has an

efficiency of 70-90% and is used from milliwatt to kilowatt applications. The Resonant Converter has an efficiency of 85-90% and is used in medium power applications.

The Power Supply used in this analysis is a particular type of SMPS called the Discontinuous Conduction Mode (DCM) Flyback Converter [7,8,9]. This is a Flyback Converter that is designed to operate in discontinuous mode. The circuit diagram of a simplified Flyback Converter is shown in Figure 1.1.

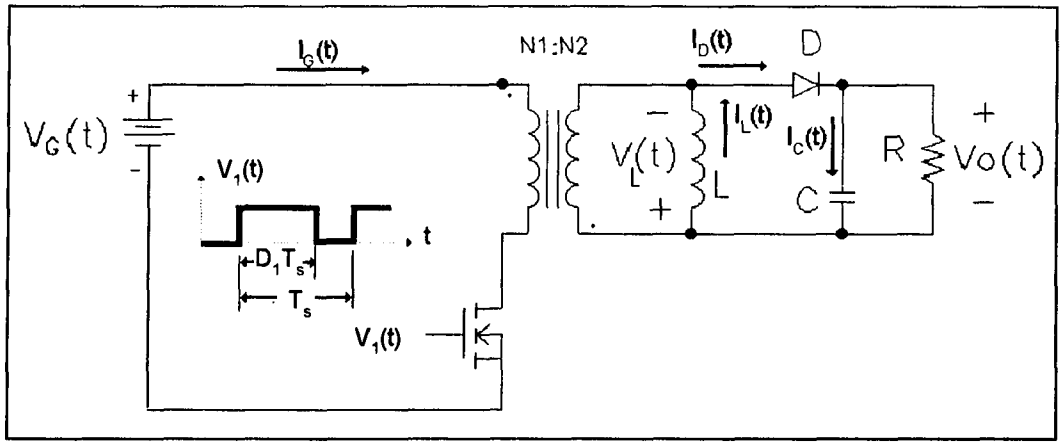

Figure 1.1-Simplified Flyback Converter

The notation used in this paper for an instantaneous voltage or current is $V_x(t)$ and $I_x(t)$, the average, (DC), voltage or current is given by V_x and I_x. It is assumed that the input and output voltage waveforms, $V_G(t)$ and $V_O(t)$, have negligible ripple so these waveforms can be approximated by their DC components V_G and V_O. The function of this type of power supply is to convert a given input voltage, $V_G(t)$, to a desired output voltage, $V_O(t)$, while supplying sufficient power to the load, R.

The mathematical relationships between the input and output voltages are a function of switching frequency, duty cycle and circuit elements. The switching frequency, f_S, is the frequency at which the transistor is cycled on and off, normally in the range of 100-200 KHz. The duty cycle, D_1, refers to the percentage of the switching period, T_S, that

the transistor is on. The duty cycle can be set for a fixed load, or it can be used as a feedback control parameter to regulate the output voltage under varying loads.

This type of power supply is useful in low power applications (200W max.) where multiple outputs or input to output isolation is required. The advantages include low parts count and accurate tracking of multiple outputs. The disadvantages include the use of a transformer instead of an inductor and the large pulsating input and output currents.

A DCM Flyback converter is a Flyback converter that is designed to operate in discontinuous mode for a portion of each switching period. Discontinuous mode is defined as a mode of operation where the current flow in the inductor is discontinuous. The other mode of operation is called Continuous Conduction Mode (CCM) where the inductor current is continuous. When the converter is operated in DCM there exists a single pole, which is easier to stabilize than the two poles and RHP zero that exist when the converter is operated in CCM. Other advantages of operating in DCM include the isolation provided by the transformer, the switch is grounded and multiple outputs can easily be incorporated.

In this application, the transformer acts like an inductor and stores energy in the primary winding in the form of a magnetic field. This transformer can be modeled as an ideal transformer with mutual inductance, L. In this application, L refers to the inductance that is seen looking back into the secondary winding of the transformer. The instantaneous inductor voltage, $V_L(t)$, becomes the voltage across the secondary of the transformer and the instantaneous inductor current, $I_L(t)$, is the current through the secondary winding of the transformer. The inductor current, $I_L(t)$, has an average (DC) component, I_L, and a ripple component, ΔI_L.

Once steady state has been reached, the operation of the DCM Flyback converter during each switching period can be separated into three distinct intervals. During the first

two intervals, the converter operates as if it were in continuous mode. In the third interval, the converter operates in discontinuous mode. The following is an analysis of the operation of the converter for each of these intervals and the resulting mathematical relationships that exists between the input and output parameters of this type of SMPS.

Interval I, $0 \le t \le D_1 \cdot T_s$

This interval begins when the controlling voltage waveform, $V_1(t)$, switches the transistor on. When the transistor is on, current flows through the primary of the transformer, through the transistor and back to the source. The input voltage, V_G, is reflected from the primary to the secondary side of the transformer, but since the diode is reversed biased, the current can not flow through the secondary winding. During this portion of the period, which lasts for $D_1 \cdot T_S$ seconds, the output capacitor supplies all of the current to the load. The design equations for this interval of the switching period are given in Equations 1.1-1.4.

$$V_L(t) = L\frac{dI_L(t)}{dt} = V_G\frac{n_2}{n_1} \tag{1.1}$$

$$I_C(t) = C\frac{dV_C(t)}{dt} = -\frac{V_O}{R} \tag{1.2}$$

$$I_G(t) = I_L(t)\frac{n_2}{n_1} \tag{1.3}$$

$$I_D(t) = 0 \tag{1.4}$$

Interval II, $D_1 \cdot T_S \le t \le (D_1 + D_2) \cdot T_S$:

The transistor is switched off by the controlling voltage waveform, $V_1(t)$. The polarity across the transformer inductor reverses in an attempt to keep the primary side current continuous; however, the transistor is off and no primary side current can flow.

Instead, the diode becomes forward biased and the energy stored in the inductor is released through the secondary winding, resulting in secondary current flow. The secondary current starts this interval at a maximum value and ramps down to zero in $D_2 \cdot T_S$ seconds. When the inductor current reaches zero, the diode prematurely shuts off. In this interval the energy is transferred to the output capacitor and to the load. The design equations for this interval of the switching period are given in Equations 1.5-1.8.

$$V_L(t) = L\frac{dI_L}{dt} = -V_O \tag{1.5}$$

$$I_C(t) = C\frac{dV_C(t)}{dt} = I_D(t) - \frac{V_O}{R} \tag{1.6}$$

$$I_G(t) = 0 \tag{1.7}$$

$$I_D(t) = I_L(t) \tag{1.8}$$

Interval III, $(D_1 + D_2) \cdot T_S \leq t \leq T_S$:

The transistor is off and the diode remains reversed biased for this portion of the switching period. The current through and the voltage across both the primary and secondary windings of the transformer are zero so there is no active transfer of energy, only the output capacitor discharging to the load. During this interval the inductor current remains at zero and the converter operates in discontinuous conduction mode. This is a function of the converter and occurs when the inductor current is designed to have a peak ripple component, ΔI_L, greater than the dc component, I_L. This results in a interval where the inductor current is held at zero by the diode. The design equations for this interval are given in Equation 1.9-1.12.

$$V_L(t) = L\frac{dI_L(t)}{dt} = 0 \tag{1.9}$$

$$I_C(t) = C\frac{dV_C(t)}{dt} = -\frac{V_O}{R} \tag{1.10}$$

$$I_G(t) = 0 \tag{1.11}$$

$$I_D(t) = 0 \tag{1.12}$$

At the end of the switching period, T_S, the voltage waveform, $V_1(t)$, turns the transistor on again and the cycle is repeated. The inductor voltage, $V_L(t)$, inductor current, $I_L(t)$, input current, $I_G(t)$, diode current, $I_D(t)$, and capacitor current, $I_C(t)$, waveforms are shown with $V_1(t)$ as the reference voltage in Figure 1.2. The mathematical relationships between the input and output parameters of the converter are obtained by applying the principles of Inductor Volt Second Balance and Capacitor Charge Balance to the equations obtained from each of the three intervals [7].

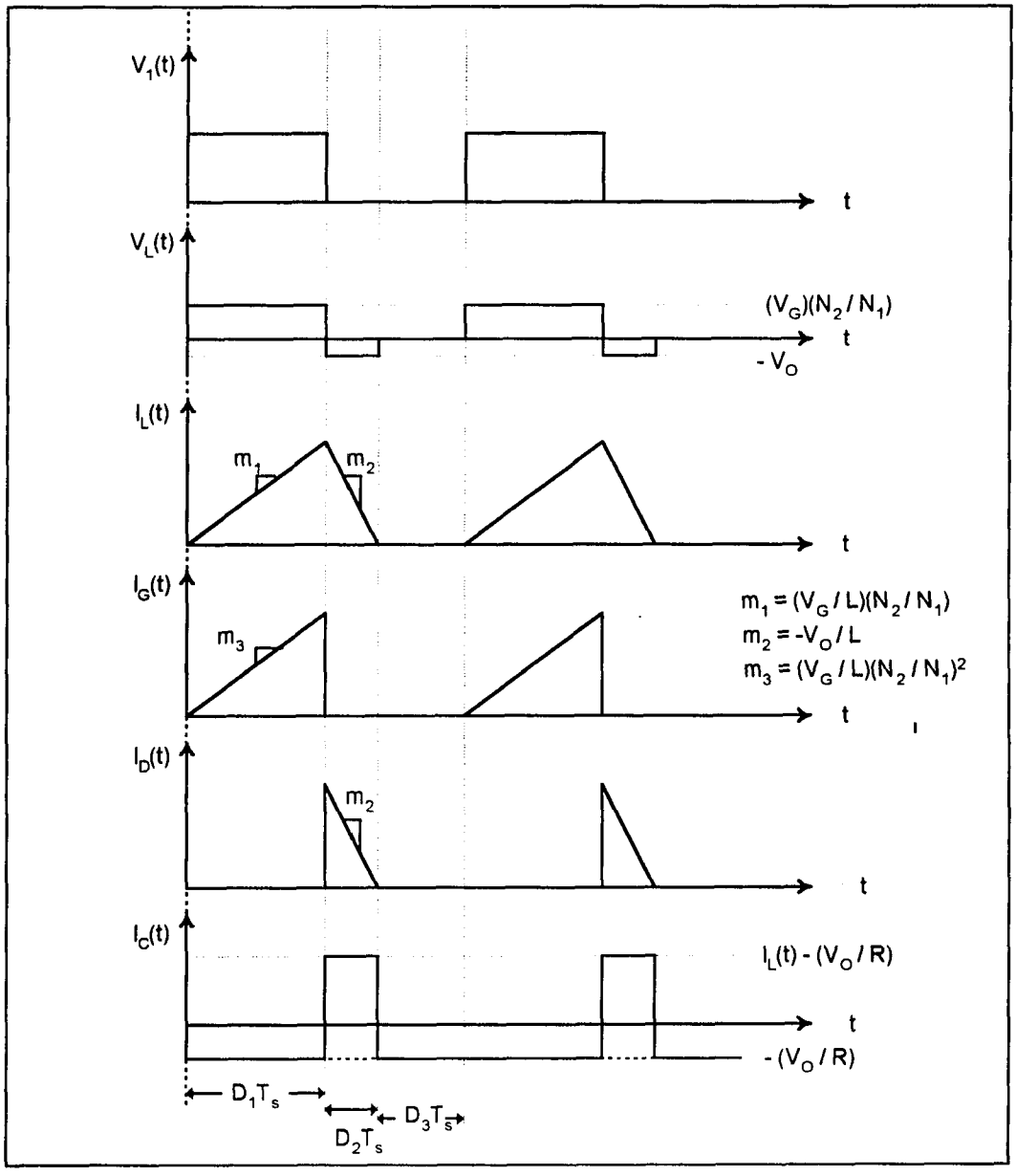

Figure 1.2-waveform diagram for a typical Flyback Converter

The principle of Inductor Volt-Second Balance states that the initial and final values of the inductor current must be equal over each switching period, or equivalently, the average (DC component) of the inductor voltage must be zero during steady state

conditions. A similar principle applies to capacitors. This is called the principle of Capacitor Charge Balance which states that the initial and final voltage across a capacitor must be equal during each switching period, or equivalently, the average (DC) capacitor current must be zero.

The output voltage, V_O, is derived by applying the principle of volt second balance to the average inductor voltage, V_L, as shown in Equations 1.13 and 1.14. The resulting Equation for V_O in terms of the input voltage, V_G, the transformer turns ratio, D_1 and D_2. is shown in Equation 1.15.

$$V_L = 0 \tag{1.13}$$

$$V_G \frac{n_2}{n_1} \cdot (D_1 \cdot T_S) - V_O \cdot (D_2 \cdot T_S) + 0 \cdot (D_3 \cdot T_S) = 0 \tag{1.14}$$

$$V_O = V_G \frac{n_2}{n_1} \frac{D_1}{D_2} \tag{1.15}$$

While V_G, the turns ratio and D_1 are inputs to the converter that can be physically set, D_2 and D_3 are non controllable converter functions. In order to derive an equation for V_O in terms of controllable parameters, Kirchoff's current law is used in Equation 1.16 to equate the average diode current, I_D, to the sum of the average capacitor current, I_C, and the average output current, V_O/R.

$$I_D = I_C + \frac{V_O}{R} \tag{1.16}$$

This relationship is simplified by applying the principle of capacitor charge balance, which states that the average capacitor current is zero. Therefore, the average diode current is equal to the average, or DC, output current shown in Equation 1.17. The mathematical expression for I_D obtained from the diode current waveform shown in Figure 1.2 is given in Equation 1.18.

$$I_D = \frac{V_O}{R} \tag{1.17}$$

$$I_D = \frac{1}{T_S}\int_0^{T_S} I_D(t)dt = \frac{1}{T_S}\left[\frac{1}{2}(V_G D_2 T_S \frac{n_2}{n_1 L})D_2 T_S\right] \tag{1.18}$$

These two equations are combined in Equation 1.19 where the output voltage is still a function of the uncontrollable parameter D_2. Equation 1.15 can be solved in terms of D_2 as shown in Equation 1.20. This equation is then substituted into Equation 1.19 and the relationship between the output voltage and the controllable parameters can be described by Equation 1.21.

$$V_O = \frac{V_G D_1 D_2 R T_S n_2}{2 L n_1} \tag{1.19}$$

$$D_2 = \frac{V_G D_1 n_2}{V_O n_1} \tag{1.20}$$

$$V_O = \frac{V_G n_2 D_1}{n_1}\sqrt{\frac{R T_S}{2L}} \tag{1.21}$$

The mathematical expressions for the peak input current and the peak diode current are also derived from Figure 1.2. The input current, $I_G(t)$, has a non zero value only during the first interval. The peak values for $I_G(t)$, and $I_D(t)$ are shown in Equations 1.22 and 1.23. Since the calculation for the peak diode current also contains the parameter D_2, Equation 1.20 is used to replace D_2 in Equation 1.23.

$$I_{Gpeak} = \frac{V_G}{L}\left(\frac{n_2}{n_1}\right)^2 D_1 T_S \tag{1.22}$$

$$I_{Dpeak} = \frac{V_O D_2 T_S}{L} = \frac{V_G D_1 T_S n_2}{n_1 L} \tag{1.23}$$

As previously stated, the DCM Flyback converter is a Flyback converter that is designed to operate in DCM. This is achieved by designing the converter in such a way

that the inductor current waveform has a DC component less than the peak ripple component. The design equations necessary to ensure DCM can be obtained by analyzing the boundary condition between the DCM and the CCM.

The inductor voltage and current waveforms of a Flyback converter are shown in Figures 1.3-1.5 for both modes of operation and for the boundary in between. Figure 1.3 shows the waveforms when the converter is operating in CCM. Note that under this mode of operation, the interval D_3 does not exist. The boundary between the two modes occurs when I_L is decreased to a value that is equal to ΔI_L as shown in Figure 1.4. As the value of I_L is decreased below the amplitude of ΔI_L, the converter enters DCM as shown in Figure 1.5.

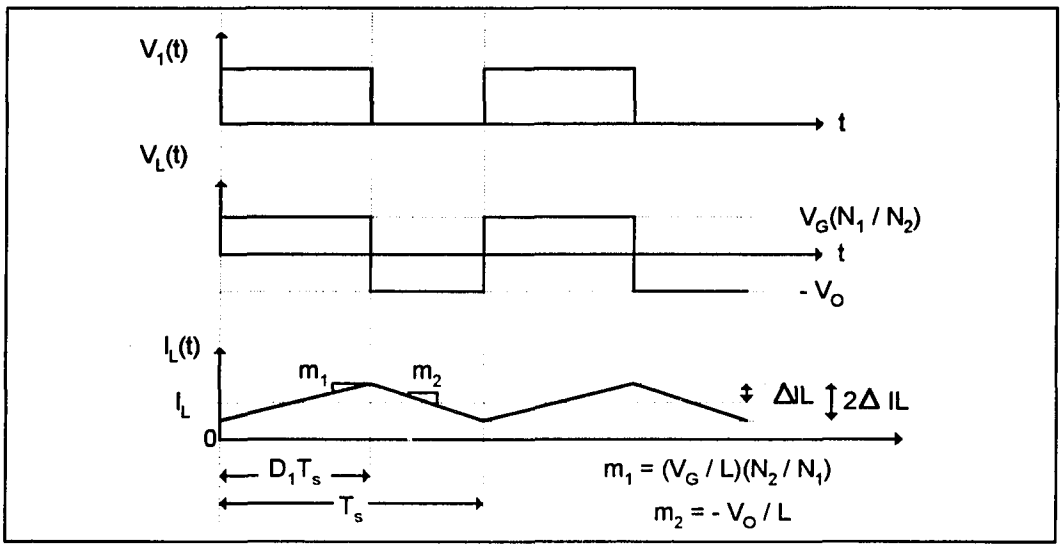

Figure 1.3-Current and voltage waveforms for inductor current in CCM

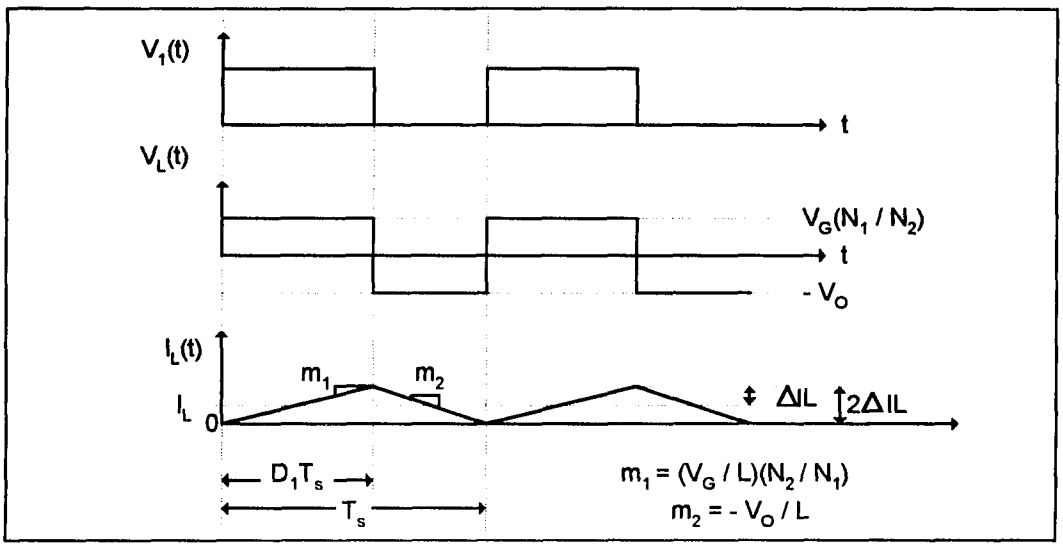

Figure 1.4-Inductor current and voltage waveforms at the boundary between CCM and DCM

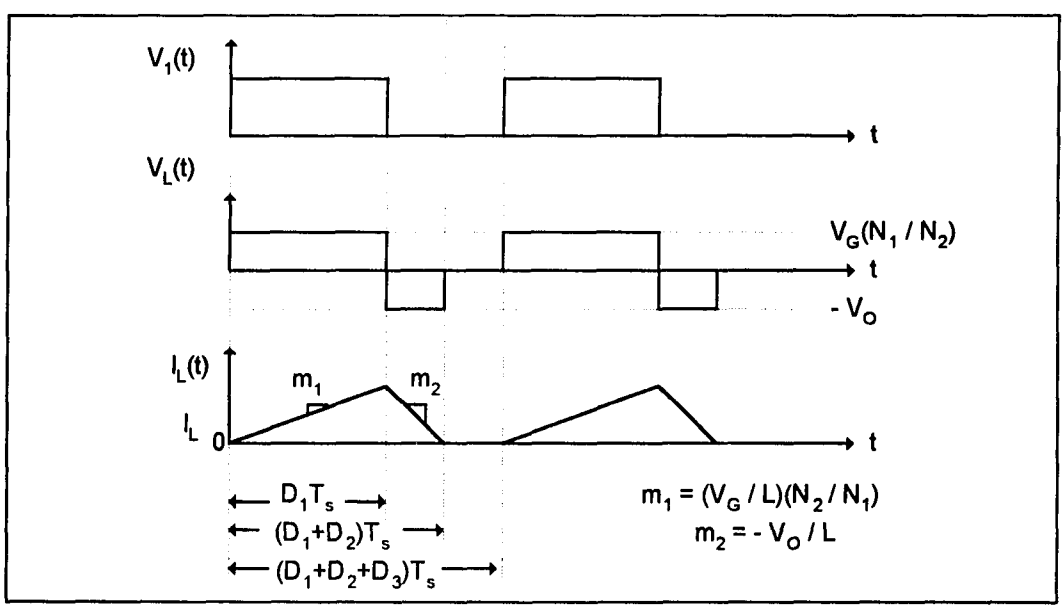

Figure 1.5-inductor current and voltage waveforms in DCM

The mathematical relationship describing the boundary between the two modes can be derived from the inductor current waveform shown in Figure 1.3 when the converter is

operating in CCM. When the converter is operated properly in this mode, the inductor current ripple, ΔI_L, is negligible compared to the DC component, I_L and the inductor current waveform $I_L(t)$ can be approximated by the DC component, I_L.

The output voltage, V_O, for continuous mode is derived by applying the principle of volt second balance to the average inductor voltage, V_L, as shown in Equations 1.24 and 1.25 where the variable D_1' is defined in Equation 1.26.

$$V_G \frac{n_2}{n_1}(D_1 T_S) - V_o(D_1' T_s) = 0 \tag{1.24}$$

$$\frac{V_O}{V_G} = \frac{n_2 D_1}{n_1 D_1'} \tag{1.25}$$

$$D_1' = (1 - D_1) \tag{1.26}$$

The average inductor current I_L is derived by applying the principle of capacitor charge balance to the capacitor current as shown in Equations 1.27 and 1.28.

$$-\frac{V_O}{R}(D_1 T_S) + I_L(D_1' T_S) - \frac{V_O}{R}(D_1' T_s) = 0 \tag{1.27}$$

$$I_L = \frac{V_O}{R D_1'} \tag{1.28}$$

The inductor current ripple, ΔI_L, is derived geometrically from $I_L(t)$ in Figure 1.4 and is given mathematically in Equation 1.29.

$$\Delta I_L = \frac{V_O D_1' T_S}{2L} \tag{1.29}$$

The boundary condition that exists between the two modes occurs when $I_L = \Delta I_L$ and is derived in Equation 1.30 from Equations 1.28 and 1.29.

$$\frac{2L}{R T_S} = (D_1')^2 \tag{1.30}$$

In order for the converter to operate in DCM, I_L must be less than ΔI_L. Equation 1.31 shows the relationship between the inductance, load resistance, duty cycle and switching period that must exist in order for the converter to operate in DCM.

$$\frac{2L}{RT_s} < (D_1')^2 \qquad (1.31)$$

1.3 EMI Generated By A DCM Flyback Converter

Electromagnetic Interference (EMI) is defined as a condition in which unintentionally transmitted electromagnetic energy generated by the operation of one piece of electronic equipment interferes with the normal operation of another piece of electronic equipment. EMI has two coupling mechanisms; radiated and conducted. The emitter, or the source, generates either radiated emissions (RE), or conducted emissions (CE). The receiver exhibits either radiated susceptibility (RS), or conducted susceptibility (CS). Examples of emitters are radio or television stations, mobile radios, CB's, computers, power lines, automobile ignition systems, radar, fluorescent bulbs and switched mode power supplies. Typical receivers include televisions, computers, audio receivers, radar navigation equipment and microwave relay stations. The amount of EMI is a measurement of the spectral energy.

There are many regulatory agencies which control EMI emissions and susceptibility both in the commercial and military sectors [10]. Most countries have their own EMI specifications and a corresponding regulatory agency. These agencies, in the commercial sector, include: FCC for the United States, VDE for Germany, and CISPR, which is the international special committee on radio interference. The purpose of these agencies is to ensure that the operation of any electronic equipment will not be impaired when subjected

to EMI, nor will it generate significant EMI, adversely affecting the operation of other pieces of electronic equipment.

The DCM Flyback Converter, like all switched mode power supplies, generates EMI that is conducted onto the power bus, V_G. This conducted EMI is generated by the input current, $I_G(t)$, which is a high frequency pulsating current. A typical military standard for this type of EMI is MIL-STD- 461C CE03, which specifies the limit of conducted EMI on a voltage bus due to a current waveform [11,12]. The frequency range of this requirement is from 15KHz to 50MHz and the emission limit is from 86dB to 20dB where dB is taken with respect to 1μ Ampere of current.

In order to determine the amount of conducted EMI generated by a DCM Flyback converter, PSPICE was used to simulate a typical DCM Flyback converter. The input current waveform, $I_G(t)$, is shown in Figure 1.6. The peak amplitude is 2.5 Amps, the switching frequency is 200KHz and the duty cycle is 50%. The high frequency sinusoidal wave that exists on this waveform is due to the leakage inductance of the transformer resonating with the parasitic capacitance of the diode.

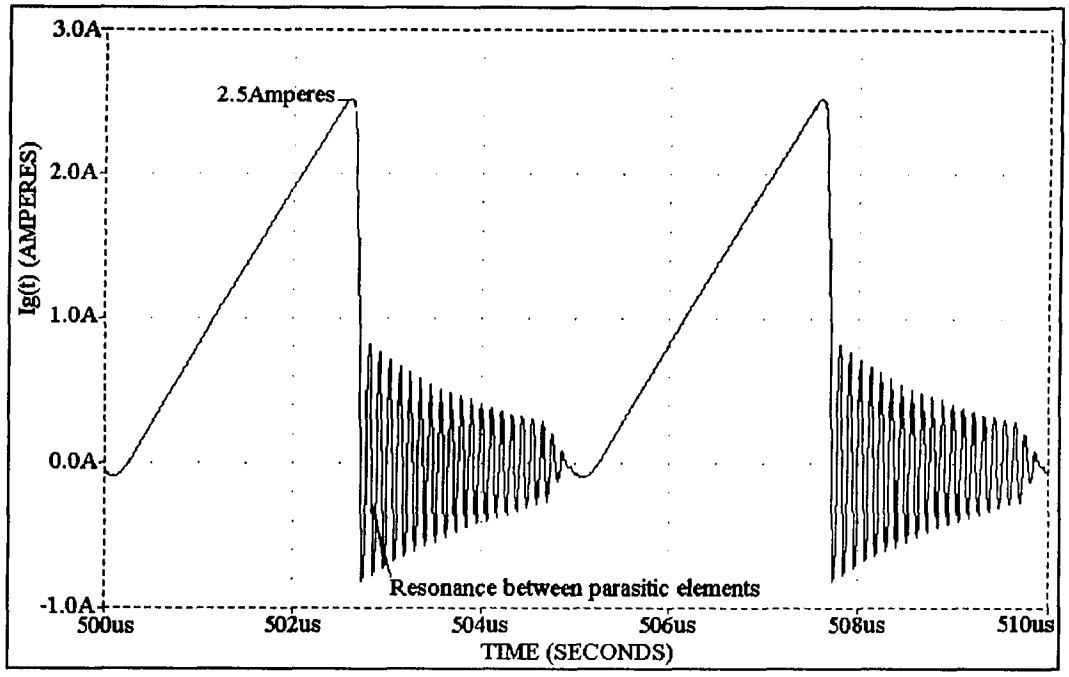

Figure 1.6-Simulated input current waveform from DCM Flyback Converter

In order to determine the amount of EMI that is conducted by $I_G(t)$, the current waveform was transformed into the frequency domain by means of a Fourier transform. The harmonic content of the input current waveform is shown in Figure 1.7 with the limit per MIL-STD-461C CE03 overlaid for comparison. The horizontal axis gives the frequency range from the fundamental frequency of 200Khz through 50Mhz. The vertical axis gives the amplitude of the frequency response of the current waveform in units of Amps. For direct comparison to MIL-STD-461, the corresponding units of dB with respect to 1μ Ampere are also given in dBμA. The conducted EMI for this particular converter is approximately 70 dB over the limit for this requirement at 200kHz. This particular SMPS requires an EMI filter with at least 70dB attenuation at the fundamental frequency to reduce the EMI to acceptable levels.

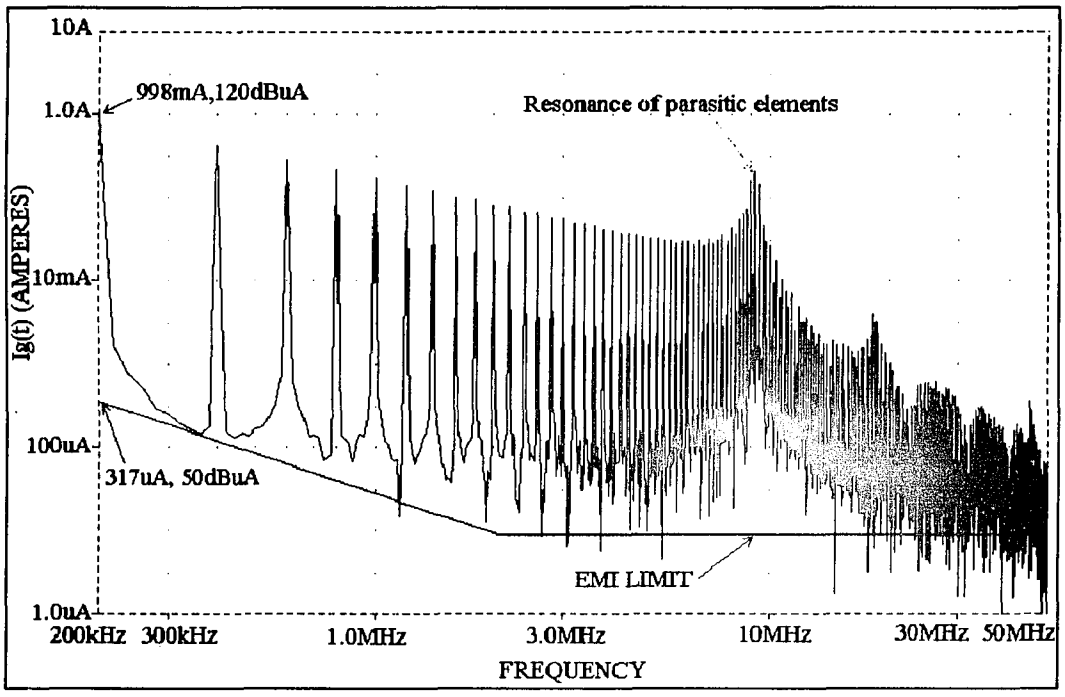

Figure 1.7-Simulated frequency spectrum of input current waveform

1.4 EMI Filter Design For A Single DCM Flyback Converter

A properly designed EMI filter that is placed between the power bus and the converter provides the attenuation necessary to reduce the current waveform, $I_G(t)$, to an acceptable level. This configuration is shown in Figure 1.8.

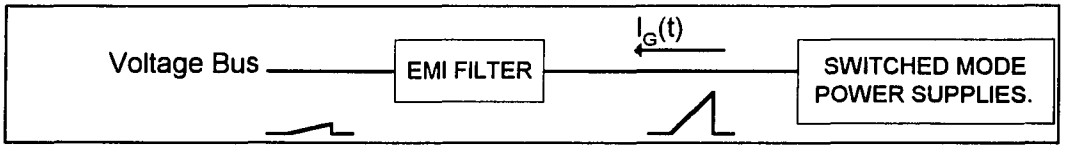

Figure 1.8-System diagram containing EMI filter

There are different types of filters that are used to reduce this type of EMI. It is sometimes necessary to separate the conducted EMI into differential and common mode parts and then incorporate specially designed components to filter each part separately. In

this work the emphasis is placed on differential mode filters like the one illustrated in Figure 1.9 [8].

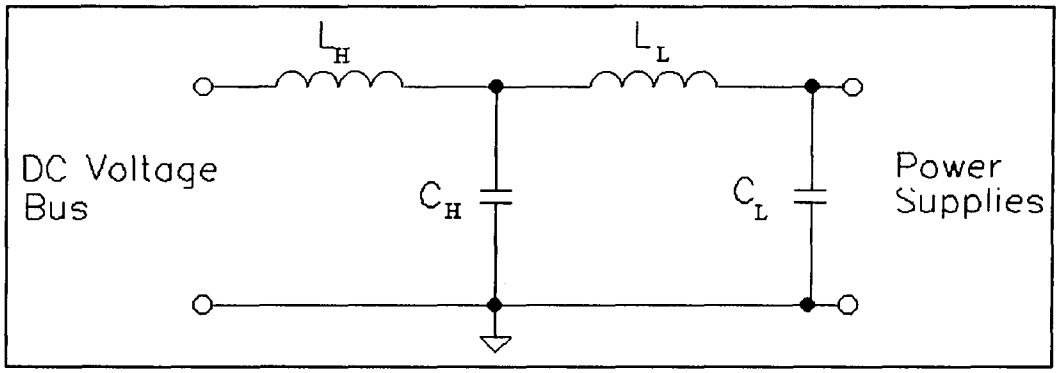

Figure 1.9-EMI filter

The LC filter utilizes the attenuation properties that are inherent to all capacitors and inductors. As the frequency increases, the attenuation of a capacitor decreases while the attenuation of an inductor increases. By choosing the appropriate number and values of inductors and capacitors, the required amount of attenuation at all frequencies can be obtained. The following is an example of the type of EMI filter that will be used in this work. In this example a filter is designed to properly attenuate the input current waveform, $I_G(t)$, generated by the single DCM Flyback converter discussed in the previous section. In order for the input current to be reduced per an EMI requirement similar to MIL-STD-461, the filter must provide at least 70 dB attenuation at the switching frequency.

Ideally, this filter could consist of the single ideal low frequency inductor and capacitor shown in Figure 1.10. This ideal filter has a gain of unity at frequencies below the cut-off frequency, f_O, and rolls off at 40 dB/dec after f_O as shown in Figure 1.11. In this Figure the switching frequency is referred to as f_S. The relationship between the cut-off frequency and the ideal inductor and capacitor values are shown in Equation 1.32.

Since the roll-off of the filter is 40dB/dec, the cut-off frequency must be located at least two decades below the switching frequency, f_S. This sets the maximum frequency for f_O at 2KHz, which in turn sets the minimum LC product at 6.33×10^{-9}. The individual values for the ideal inductor and capacitor may be determined by other design constraints or component availability. One possible combination of ideal components is a 29uH inductor with a 220uF capacitor. This combination provides an attenuation of 80 dB at the switching frequency of 200Khz which gives a 10dB margin for error. Since the attenuation of the ideal filter increases and the amplitude of the harmonic content of the input current waveform decreases as the frequency increases, the filter will provide sufficient attenuation for all frequencies.

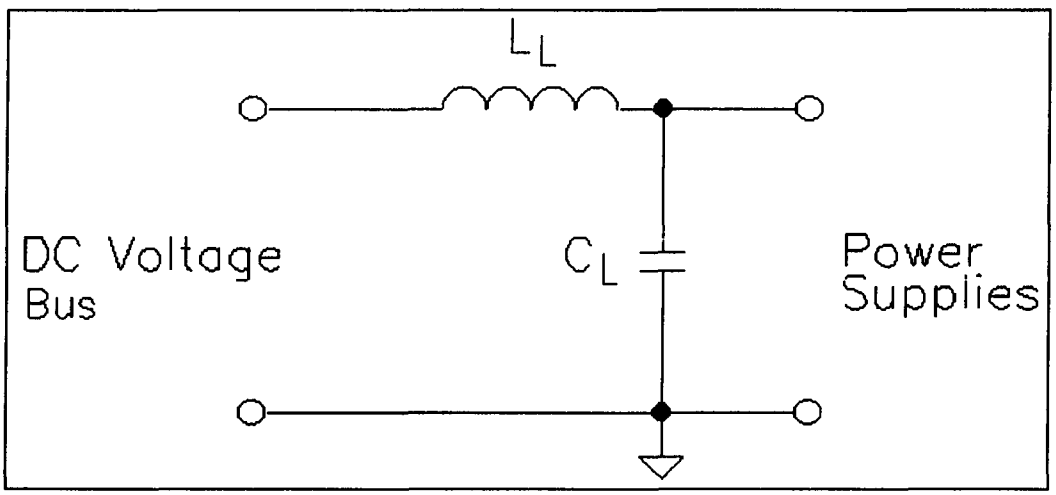

Figure 1.10-simplified ideal EMI filter

$$f_o = \frac{1}{2\pi\sqrt{LC}} \qquad (1.32)$$

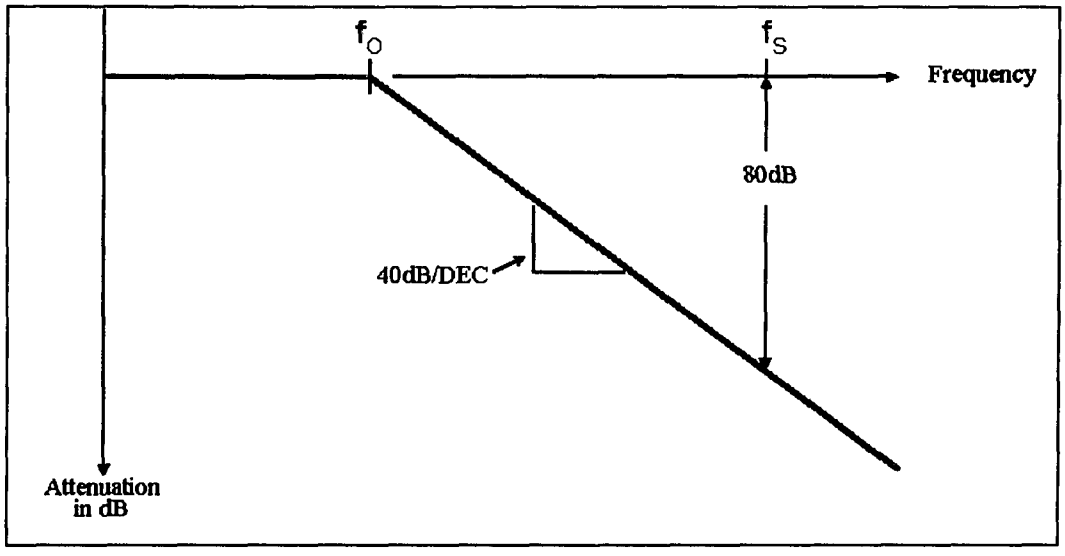

Figure 1.11-Attenuation of the ideal filter shown in Figure 1.10

In reality, ideal components do not exist. Capacitors and inductors contain parasitic elements. These parasitic elements are a function of the physical design of the components and cause non ideal behavior of the component over frequency. The attenuation of a capacitor is a function of the capacitance and parasitic elements. The capacitor behaves like a capacitor only for a limited frequency range, for other frequencies it behaves like an inductor or a resistor. Similarly, an inductor behaves like an inductor, a capacitor and a resistor at different frequencies. These parasitic elements can result in an unacceptable decrease in attenuation at various frequencies.

In order to compensate for these parasitic elements, a low frequency capacitor and inductor are used to start the filter attenuation at 40 dB/dec and a high frequency capacitor and inductor are added to compensate for the parasitic elements of the low frequency capacitor and inductor like the filter shown in Figure 1.9.

1.5 System Description

The system used to illustrate the effect that the phase relationship between individual DCM Flyback converters has on the total EMI conducted onto the power bus is shown in Figure 1.12. This system consists of multiple SMPS which are connected in parallel to a single DC voltage bus. The SMPS are DCM Flyback converters operating at the same switching frequency.

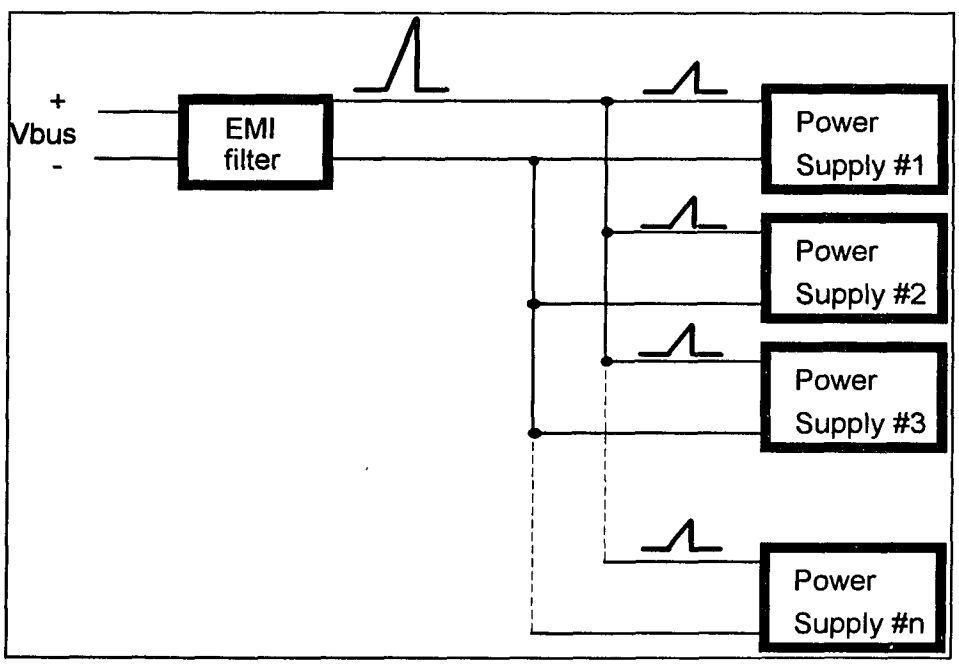

Figure 1.12-System of multiple SMPS operating on a single voltage bus.

The individual current waveforms combine on the DC power bus in various ways depending upon the phase relationships that exist between them. If all the converters are switched on at exactly the same time, the combined current will have a peak amplitude equal to the sum of the individual peaks. In this case the resultant EMI is maximum. However, if the converters are switched on at different times, the shape and amplitude of the combined waveform would be much different and the resultant EMI smaller.

The goal of this work is to determine the optimal phase relationship between the DCM Flyback converters of this system that will result in a minimal amount of EMI being conducted onto the voltage bus. Once this amount is determined, an optimal EMI filter can be designed to bring the remaining EMI down to acceptable levels.

CHAPTER 2

ANALYSIS AND SIMULATION OF THE REDUCTION OF EMI

2.0 Introduction

In this chapter the system of Chapter 1 is simplified to the extent that the SMPS have identical switching frequencies and the input current waveforms are modeled by ideal triangular waveforms. These triangular waveforms provide a simple and accurate model for the input current waveforms, $I_G(t)$, generated by the DCM Flyback SMPS. The conducted EMI of this system is reduced by optimizing the phase relationship between input current waveforms generated by the individual converters. Since the amount of EMI is measured by transforming the combined input current waveform from the time domain into the frequency domain by a Fourier transform, a review of this type of transformation is also presented. It is then shown that given a system of n identical SMPS with triangular input current waveforms, the amount of conducted EMI is minimized when the phase shift between each input current waveform is equal 360°/n.

The same method of reducing the amount of EMI is applied to a system where the individual input current waveforms have the same switching frequency but have variations in amplitudes or duty cycles. It is shown that the amount of conducted EMI is minimized even if there exist small variations between individual converters. This is true as long as the switching frequency is the same for each SMPS and the phase shift between the individual input current waveforms is equal to the switching period divided by the number of converters in the system.

2.1 Equivalent Model for Input Current of DCM Flyback Converter

A PSPICE simulation of a DCM Flyback converter similar to the one shown in Figure 1.1 generates the input current waveform, $I_G(t)$, shown in Figure 1.6. The peak

amplitude is 2.5 Amperes, the duty cycle is set at 50% and the switching frequency is 200kHz. The interval shown begins after the converter has reached steady state at 500μ seconds and continues for two switching periods. The Fourier transform of this waveform is shown in Figure 1.7. This frequency transformation determines the harmonic magnitude of $I_G(t)$ at every frequency that is a multiple of the fundamental frequency. The fundamental frequency is the lowest frequency component that is contained in $I_G(t)$, in this case it is the switching frequency, 200kHz.

To fully understand how waveforms of this type combine in the frequency domain, it is necessary to symbolically derive the Fourier Transformation of a single waveform. Since the waveform of Figure 1.6 is too complicated for such an analysis, an equivalent model is developed. This waveform has low frequency components due to the basic triangular waveform and higher frequency components due to the resonance between the parasitic diode capacitance and the leakage inductance of the transformer within the converter. This can be seen from the frequency spectrum shown in Figure 1.7. In order to simplify the model, the high frequency components generated by the DCM Flyback converter are neglected and $I_G(t)$ is approximated by the ideal triangular current waveform shown in Fig. 2.1.

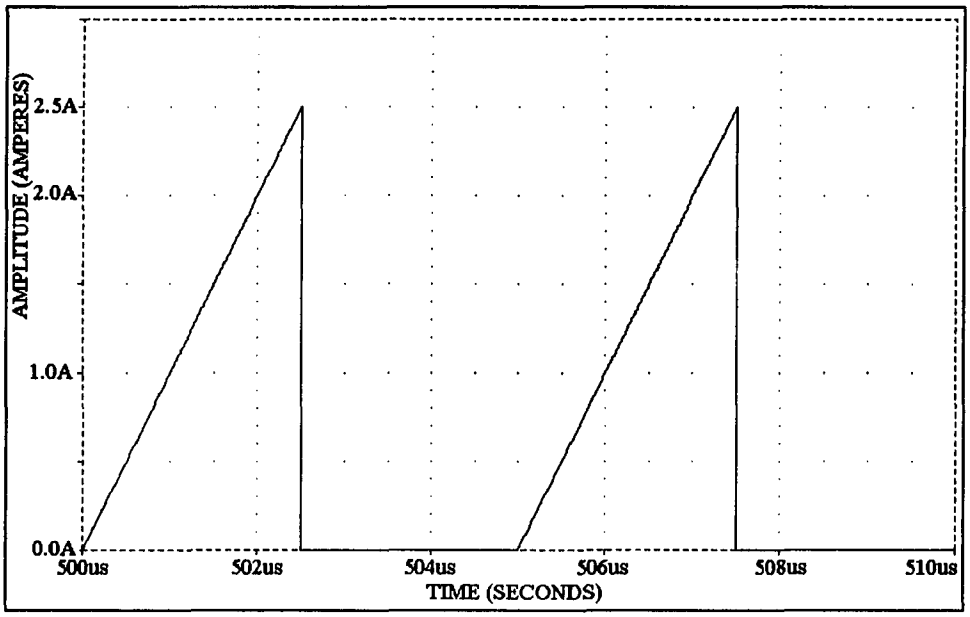

Figure 2.1-Ideal triangular waveform

To verify this approximation in the frequency domain, a Fourier Transform of the ideal triangular current waveform of Figure 2.1 is performed using PSPICE. The frequency content of this waveform is shown in Figure 2.2. A comparison of the frequency content of this ideal triangular waveform and the input current generated by the simulated DCM Flyback converter is shown in Figure 2.3. Here it can be seen that the two waveforms have similar harmonic magnitudes at the lower frequencies. The simulated DCM Flyback converter has a peak at about 10MHz where the transformer leakage inductance resonates with the parasitic capacitance of the diode. The ideal triangular waveform has larger high frequency components since it has a sharper peak than the simulated waveform generated by the DCM Flyback converter.

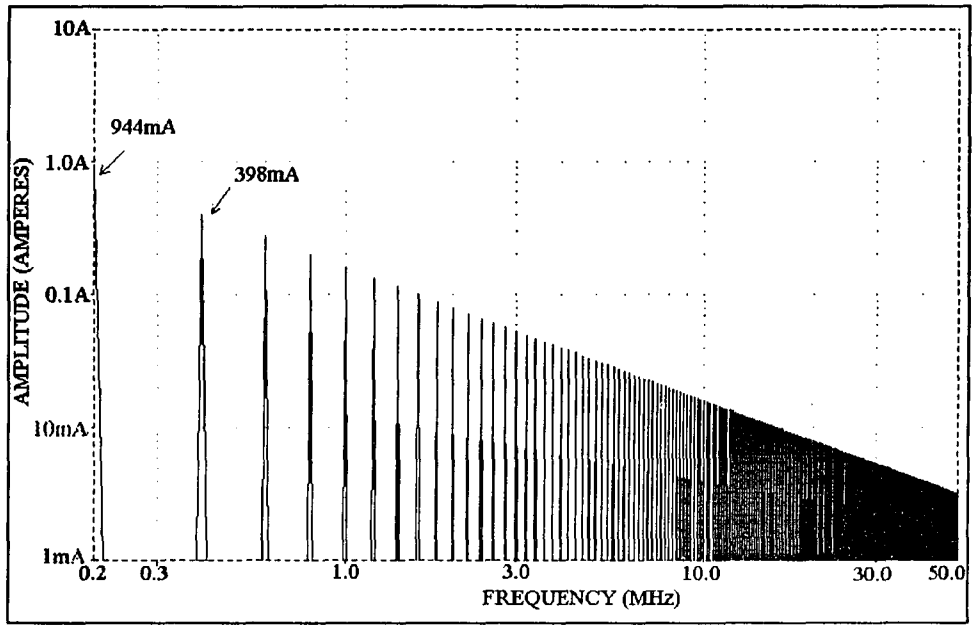

Figure 2.2-Frequency spectrum of ideal triangular waveform

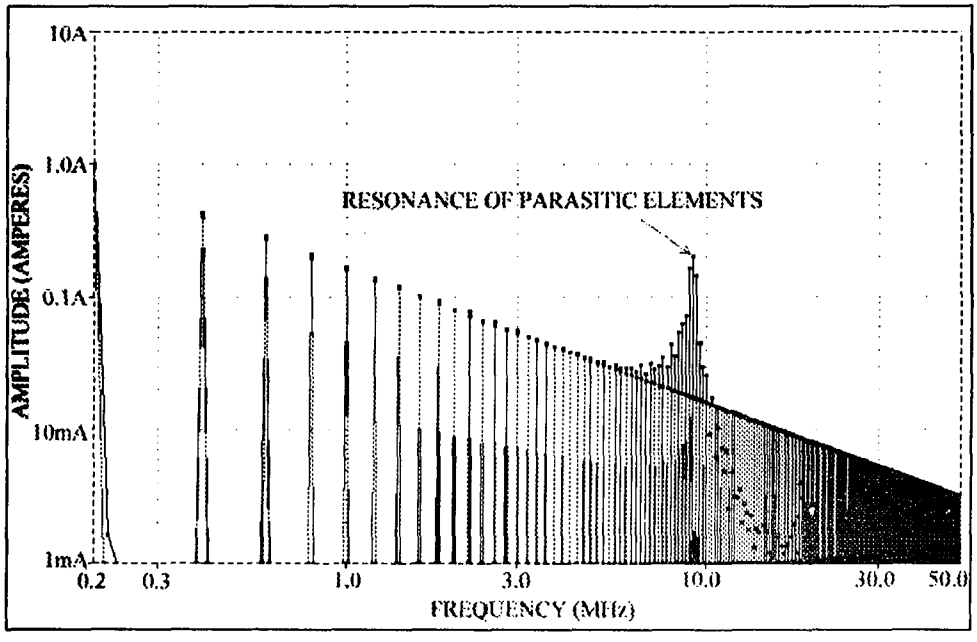

Figure 2.3-Frequency spectra of ideal triangular waveform and input current waveform generated by simulated DCM Flyback Converter

The ideal triangular waveform is an acceptable model for the simulated input current waveform, $I_G(t)$, generated by a DCM Flyback converter, at least as far as the frequency domain analysis of the EMI filter is concerned. The EMI filter is designed to provide a specific amount of attenuation at the fundamental frequency. Since the harmonic magnitude of this type of waveform decreases as frequency increases, a good EMI filter also provides sufficient attenuation at frequencies above the fundamental frequency. Because of this the higher frequency components of the waveform can be neglected.

2.2 Trigonometric Form of the Fourier Series For Triangular Waveforms

Before the optimum phase relationship between the input current waveforms generated by multiple converters can be found, the frequency content of a single input current waveform, $I_G(t)$, is derived. This is necessary to determine how these input current waveforms combine in the frequency domain. As shown in the previous section, $I_G(t)$ can be modeled as the ideal triangular waveform, *f(t)* of Figure 2.4. The x-axis is time in seconds. The period, T, is the interval (t_0,t_3) and the duty cycle is defined as $(t_2-t_1)/T$. The y-axis is amplitude in Amperes with the peak amplitude given as the variable A. Since this is a periodic waveform, a Fourier Transform can be used to transform the waveform into the frequency domain and compute the amplitude at each of the harmonic frequencies. The following is a review of the Fourier transform using the Fourier Series representation of a periodic waveform [13,14].

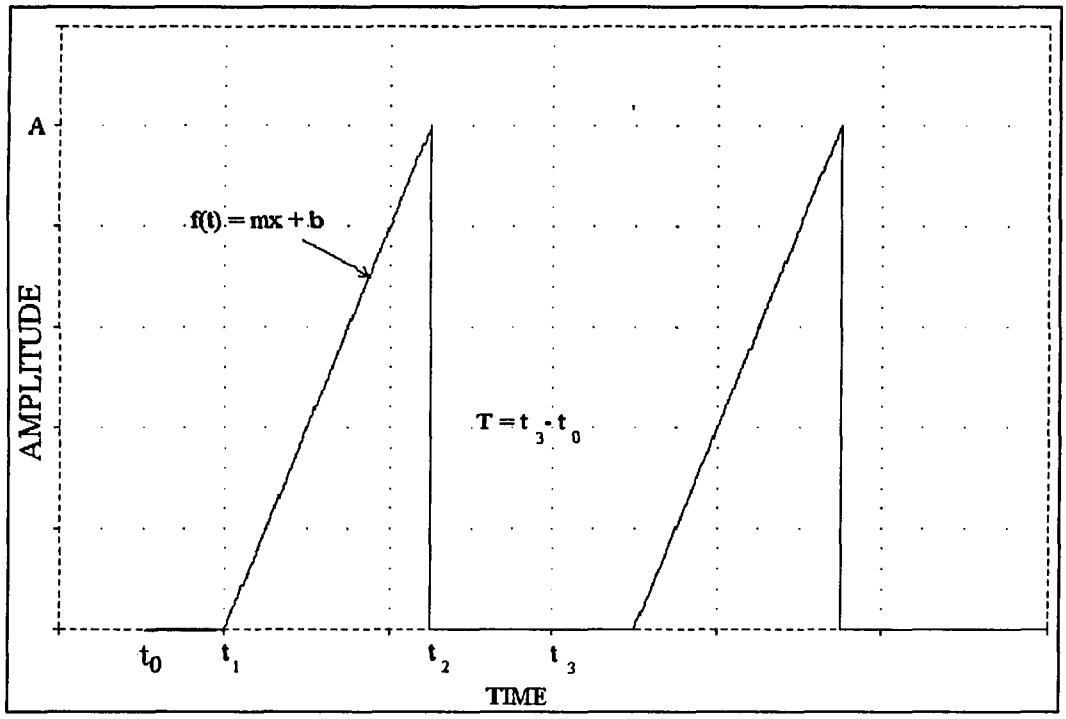

Figure 2.4-Generalized Ideal Triangular Waveform

The Fourier Transform of the waveform of Figure 2.4 can be obtained by representing the time varying waveform by an equivalent Fourier series representation. The equation of the Fourier series representation of a periodic function is given by $f(t) = a_0 + \sum_{n=1}^{\infty} a_n \cos n\omega t + \sum_{n=1}^{\infty} b_n \sin n\omega t$, where $\omega=2\pi/T$ and T is the period of the waveform. The coefficients a_0, a_n and b_n are given in Equations 2.1-2.3 and the magnitude of each harmonic is given as c_n in Equation 2.4.

$$a_0 = \frac{1}{T}\int_0^T f(t) \tag{2.1}$$

$$a_n = \frac{2}{T}\int_0^T f(t)\cos n\omega t dt \tag{2.2}$$

$$b_n = \frac{2}{T}\int_0^T f(t)\sin n\omega t dt \tag{2.3}$$

$$c_n = \sqrt{a_n^2 + b_n^2} \tag{2.4}$$

The function, $f(t)$, has a non-zero value only during the interval from t_1 to t_2 where it is defined by the equation of a line, $f(t) = mx + b$. In order to simplify the calculations of the Fourier coefficients, the integrals were solved symbolically and the resulting equations are shown in Equations 2.5-2.8.

$$a_0 = \frac{1}{T}\left(\frac{m}{2}\left(t_2^2 - t_1^2\right) + b\left(t_2 - t_1\right)\right) \tag{2.5}$$

$$a_n = \frac{2}{T}\left[\begin{array}{l}\frac{m}{(n\omega)^2}\left(\cos n\omega t_2 - \cos n\omega t_1 + n\omega\left(t_2 \sin n\omega t_2 - t_1 \sin n\omega t_1\right)\right) \\ + \frac{b}{(n\omega)}\left(\sin n\omega t_2 - \sin n\omega t_1\right)\end{array}\right] \tag{2.6}$$

$$b_n = \frac{2}{T}\left[\begin{array}{l}\frac{m}{(n\omega)^2}\left(\sin n\omega t_2 - \sin n\omega t_1 - n\omega t_2 \cos n\omega t_2 + n\omega t_1 \cos n\omega t_1\right) - \\ \frac{b}{n\omega}\left(\cos n\omega t_2 - \cos n\omega t_1\right)\end{array}\right] \tag{2.7}$$

$$c_n = \sqrt{a_n^2 + b_n^2} \tag{2.8}$$

2.3 EMI Of A System Of Two DCM Flyback Converters

Consider the system of Figure 2.5 which consists of two DCM Flyback converters. The input current waveforms, $I_G(t)$, are simplified to the extent that they have identical periods, duty cycle and peak amplitude. It is also assumed that the timing between the two waveforms can be controlled. The period is 5μ second for a switching frequency of 200KHz, the duty cycle is 50% and the amplitude is 1.0 Ampere.

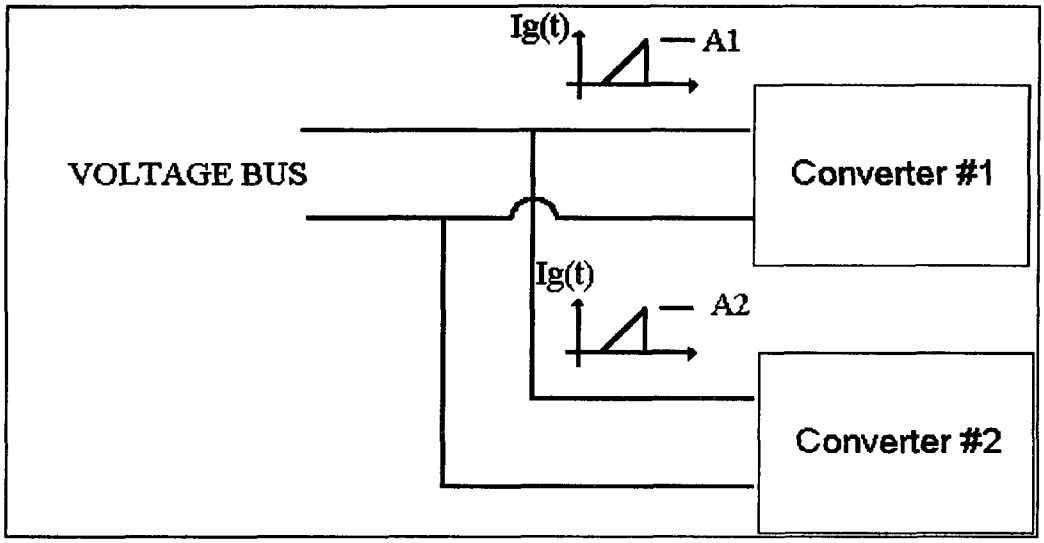

Figure 2.5-System of two DCM Flyback Converters

The following analysis investigates the effect that phase relationships between two input current waveforms have on the amount of system EMI. The first case is where the two waveforms are combined with a phase shift of 0°. The second case is where the same waveforms are combined with a phase shift of 180°. This is followed by a comparison of the harmonic spectrum of the EMI that results from the two phasing conditions.

2.3.1 EMI Generated By Two Waveforms With A Phase Shift Of 0°

The modeled input current, $I_G(t)$, of converter #1 is shown in Figure 2.6 switching on at t=0 sec and reaching a peak value of 1.0 Ampere at the end of the duty cycle at 2.5 μsec., at this point the waveform switches off and remains at zero for the rest of the cycle before switching on again. Substituting $t_0=t_1=0$, $t_2=2.5\mu$ second, $t_3=5\mu$ second and A=1.0 Ampere into Equations 2.6 and 2.7, the coefficients a_n and b_n are derived as shown in Equations 2.9 and 2.10. The magnitude of each nth harmonic is given by Equation 2.8 and is plotted in Figure 2.7. The dc component given by the coefficient a_0, does not contribute to the harmonic magnitude so it is not included in this analysis.

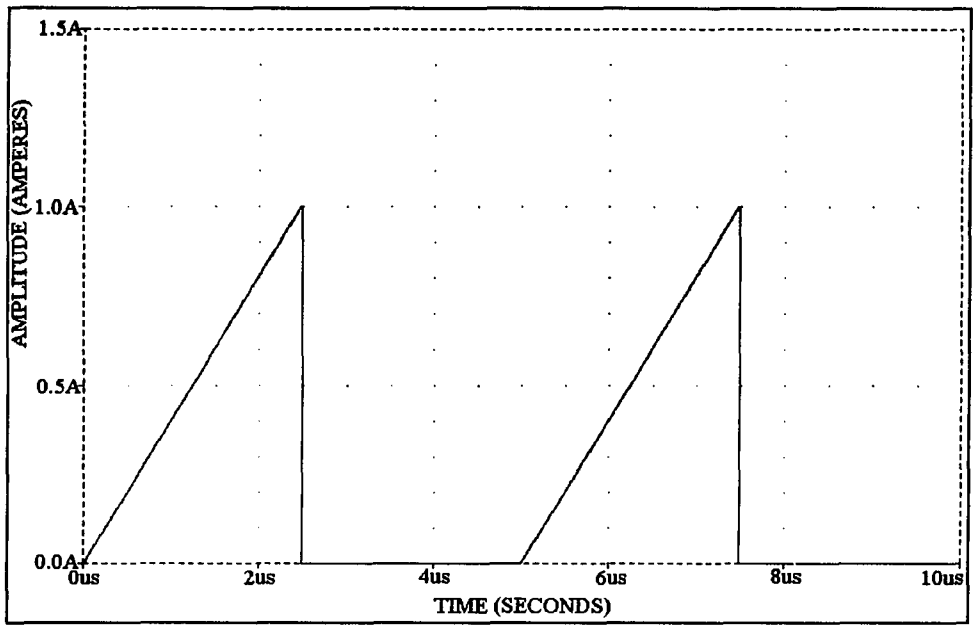

Figure 2.6-Ideal input current waveform

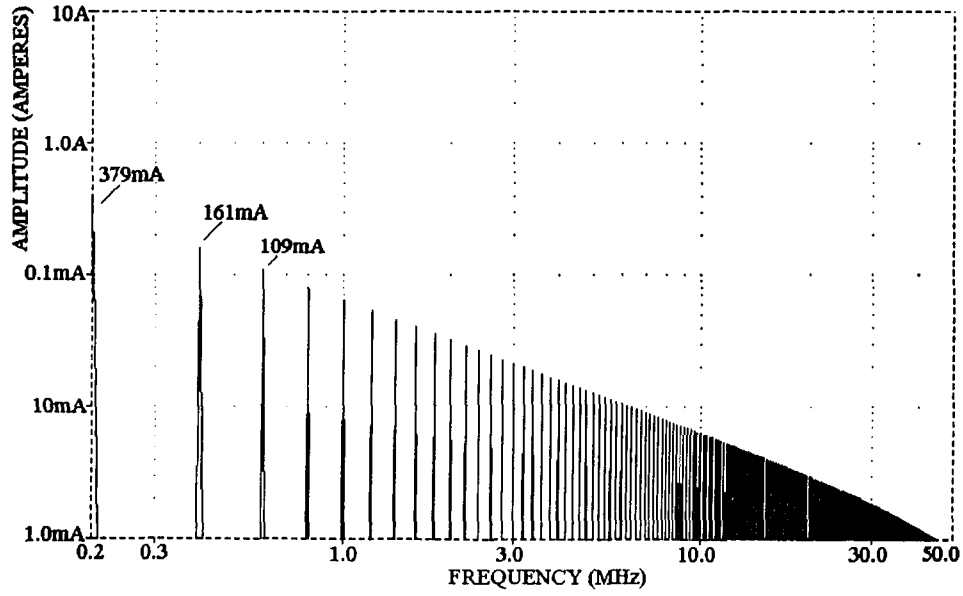

Figure 2.7-Harmonic Spectrum of the single triangular waveform of Figure 2.6

$$a_n = -\frac{2}{(n\pi)^2} \text{ if } n \text{ is odd and 0 if } n \text{ is even} \qquad (2.9)$$

$$b_n = \frac{1}{n\pi} \text{ if } n \text{ is odd and } -\frac{1}{n\pi} \text{ if } n \text{ is even} \qquad (2.10)$$

If converter #2 is switched on at the same time as converter #1, the two waveforms combine as shown in Figure 2.8. The resultant Fourier coefficients of the input current waveform of converter #2 are identical to Equations 2.9 and 2.10. The combined Fourier coefficients, a_n and b_n, of the two waveforms are obtained by multiplying the coefficients of Equations 2.9 and 2.10 by two and are given in Equations 2.11 and 2.12. Again the magnitude of each harmonic is calculated using Equation 2.8 which reduces to Equation 2.13 and is shown in Figure 2.9.

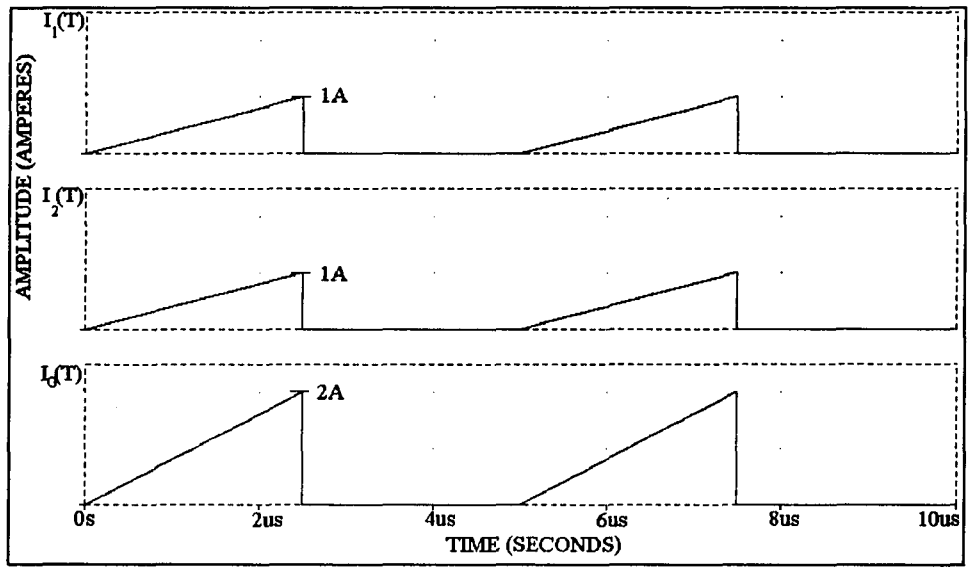

Figure 2.8-Two ideal input current waveforms combined with a phase shift of 0°.

$$a_n = -\frac{4}{(n\pi)^2} \text{ if } n \text{ is odd and 0 if } n \text{ is even} \qquad (2.11)$$

$$b_n = \frac{2}{n\pi} \text{ if } n \text{ is odd and } -\frac{2}{n\pi} \text{ if } n \text{ is even} \qquad (2.12)$$

$$c_n = \sqrt{\left(\frac{4}{(n\pi)^2}\right)^2 + \left(\frac{2}{n\pi}\right)^2} \text{ if n is odd, and}$$

$$= \frac{2}{n\pi} \text{ if n is even} \qquad (2.13)$$

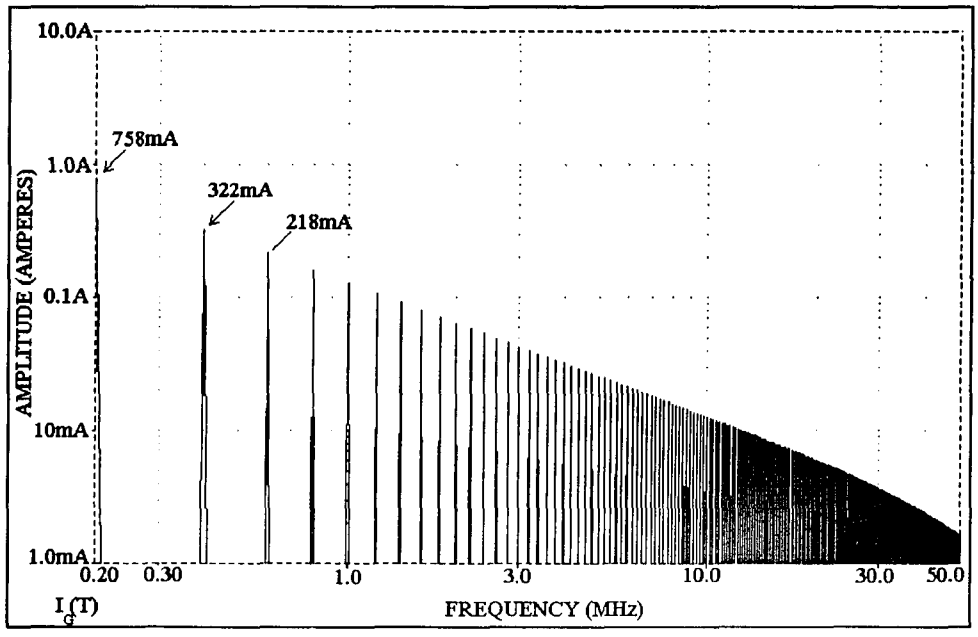

Figure 2.9-The harmonic spectrum of $I_G(t)$ when two ideal waveforms are combined with a phase shift of 0°

In this case, the harmonic spectrum of the combined waveforms has the same fundamental frequency as the single converter but it has twice the magnitude at each harmonic. This can be seen by comparing the frequency spectrum of $I_G(t)$ from the single converter in Figure 2.7 to the frequency spectrum of the combined current waveform in Figure 2.9.

2.3.2 EMI Generated By Two Waveforms With A Phase Shift of 180°

In this section the resultant harmonic spectrum of the system of Figure 2.5 is examined when the two waveforms are combined 180 degrees out of phase. The individual waveforms and the timing relationships are shown in Figure 2.10. The top waveform starts to ramp up at zero seconds and reaches the peak value of 1.0 Ampere at 2.5μ second. At this time the waveform drops back to zero and remains there for the remainder of the switching period. The Fourier coefficients for this waveform are also given by Equation 2.9 and 2.10. The middle waveform, which is the input current from converter #2, remains at zero until 2.5μ second and then ramps up to 1.0 Ampere during the remainder of the switching period. The Fourier coefficients for this waveform are derived using Equations 2.6 and 2.7 and are given in Equation 2.14 and 2.15.

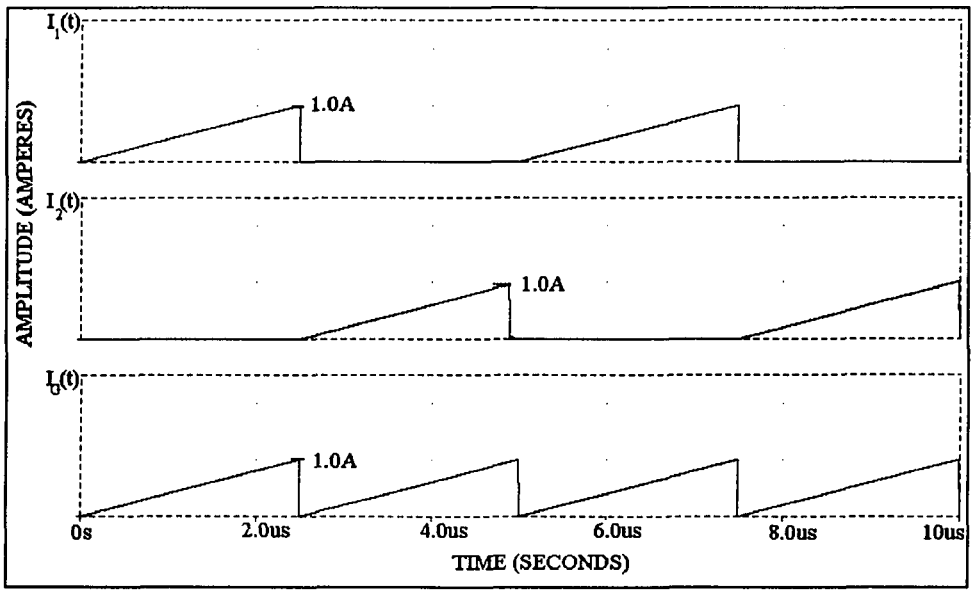

Figure 2.10-Two ideal input current waveforms combined with a phase shift of 180°.

$$a_n = \frac{2}{(n\pi)^2} \text{ if } n \text{ is odd and 0 if } n \text{ is even} \qquad (2.14)$$

$$b_n = \frac{1}{n\pi} \text{ if } n \text{ is odd and } \frac{-1}{n\pi} \text{ if } n \text{ is even} \qquad (2.15)$$

The waveform on the bottom of Figure 2.10 is the combined current waveform. The Fourier coefficients of this waveform are derived from Equations 2.9, 2.10, 2.14 and 2.15 and are given in Equation 2.16 and 2.17. The magnitude of each harmonic is given by Equation 2.18 and is shown graphically in Figure 2.11.

$$a_n = 0 \qquad (2.16)$$

$$b_n = 0 \text{ if } n \text{ is odd and } \frac{-2}{n\pi} \text{ if } n \text{ is even} \qquad (2.17)$$

$$c_n = \frac{2}{n\pi} \text{ if } n \text{ is even and 0 if } n \text{ is odd} \qquad (2.18)$$

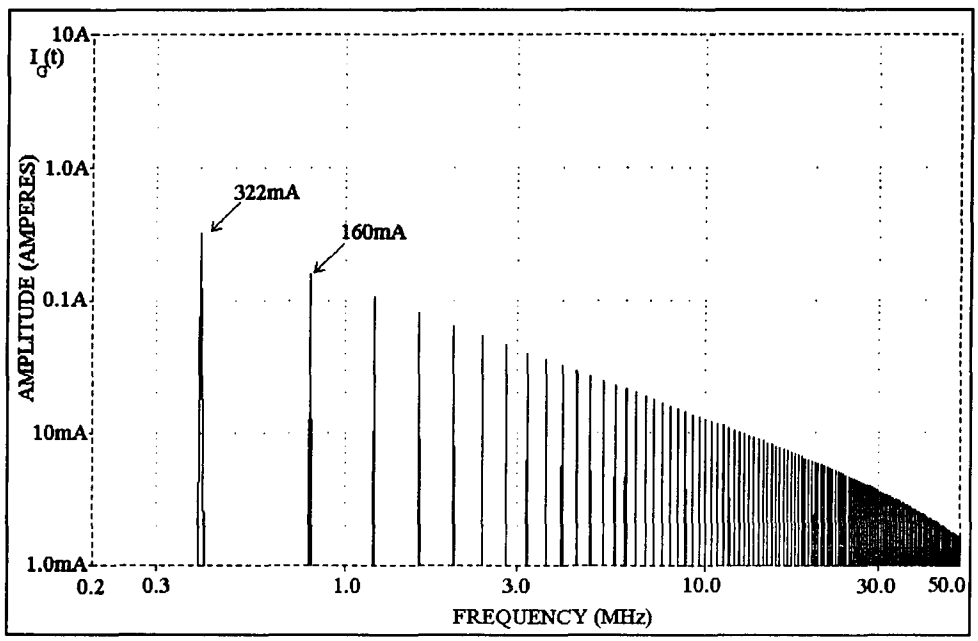

Figure 2.11-Spectral content of two identical waveforms combined with a phase shift of 180°.

In this case, the current waveforms combine in such a way that the fundamental and all odd harmonics cancel, the magnitude of the even harmonics remain the same and the fundamental frequency moves from 200KHz to 400KHz.

2.3.3 Comparison Of System EMI Generated By Two Waveforms Combined with 0° and 180° Phase Shifts

The advantage that doubling the fundamental frequency has on the filter design can be seen by comparing the two frequency spectrums shown in Figures 2.9 and 2.11. In order to meet EMI requirements given in Chapter 1.3, the waveform shown in Figure 2.9 must be reduced by approximately 67dB at 200KHz and the waveform of Figure 2.11 must be reduced by approximately 68 dB at 400KHz. This requires a filter with an LC product of 6.3 X 10^{-13} and 1.5X10^{-13} respectively. The LC products are derived from Equation 2.19, where L and C are the low frequency filter elements and f_s is the appropriate fundamental frequency.

$$f_s = \frac{1}{2\pi\sqrt{LC}} \qquad (2.19)$$

When the two waveforms are combined with a phase shift of 180° the EMI filter LC product can be one fourth of the value needed to provide the same filtering for the case where the waveforms are coincident. The advantages of using smaller valued filter components becomes apparent when selecting the inductor. The smaller the value of the inductor, the smaller the physical size, the more current the inductor can carry without saturating and the smaller the cost.

2.4 EMI Of A System Of Three DCM Flyback Converters

It has been determined analytically in the previous section that the fundamental frequency of a system containing two identical converters can be increased by a factor of

two if the two waveforms are combined 180 degrees out of phase with each other. This naturally leads to the question of what optimal phase relationship exists for a system that contains three identical converters. The block diagram of this system is shown in Figure 2.12.

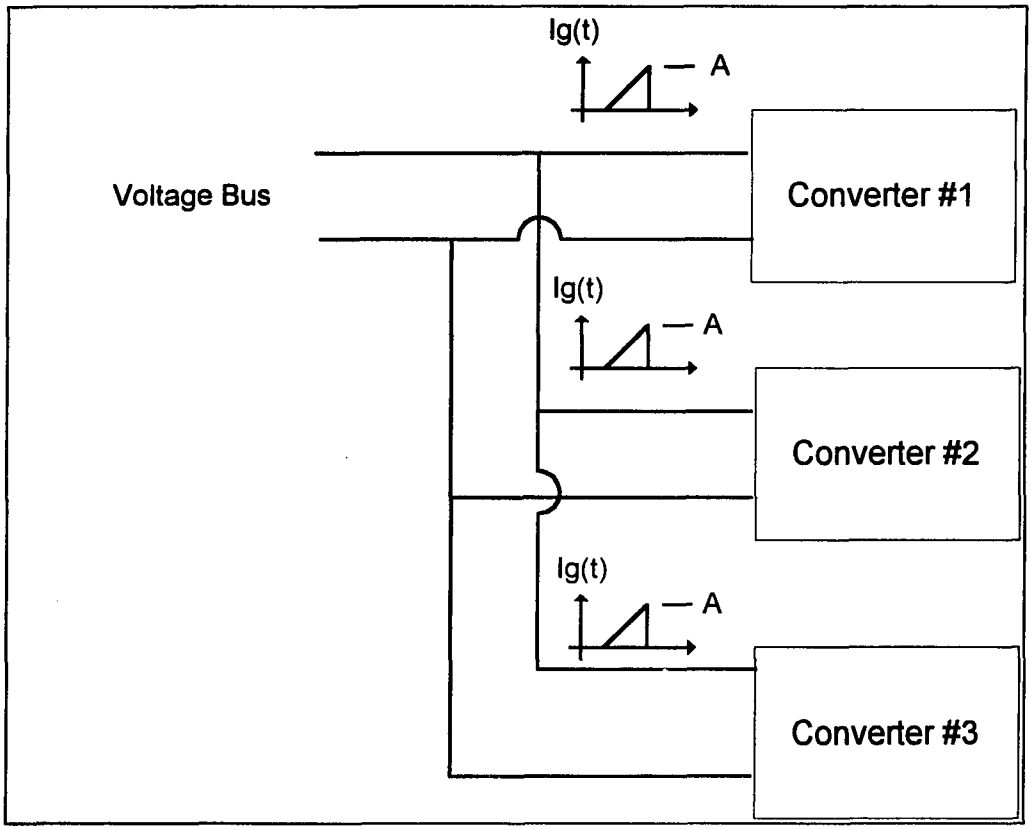

Figure 2.12-Block diagram of system of three identical converters

In order to see how the phase relationships between the individual converters effect the combined frequency spectrum of the system, various timing schemes are imposed on the individual input current waveforms. The condition where the three waveforms are combined with a phase shift of 0° is shown in Figure 2.13, the combined current being the

bottom waveform. Again, the individual current waveforms have a switching frequency of 200kHz, duty cycle of 50% and a peak amplitude of 1.0 Ampere.

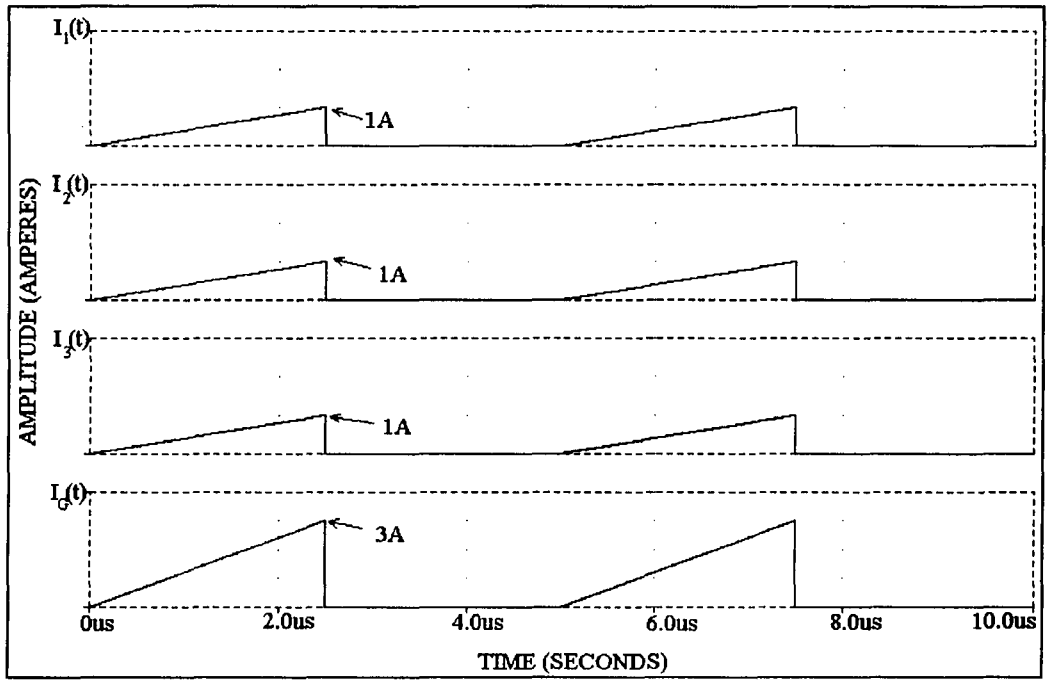

Figure 2.13-Three identical waveforms combined with a phase shift of 0°.

The harmonic content of the combined waveform can be derived from Equations 2.6-2.8 with the resulting frequency spectrum of Figure 2.14. The fundamental frequency is 200kHz which is the switching frequency of the converter. In this case, the amplitude of the harmonics are three times that of a single converter.

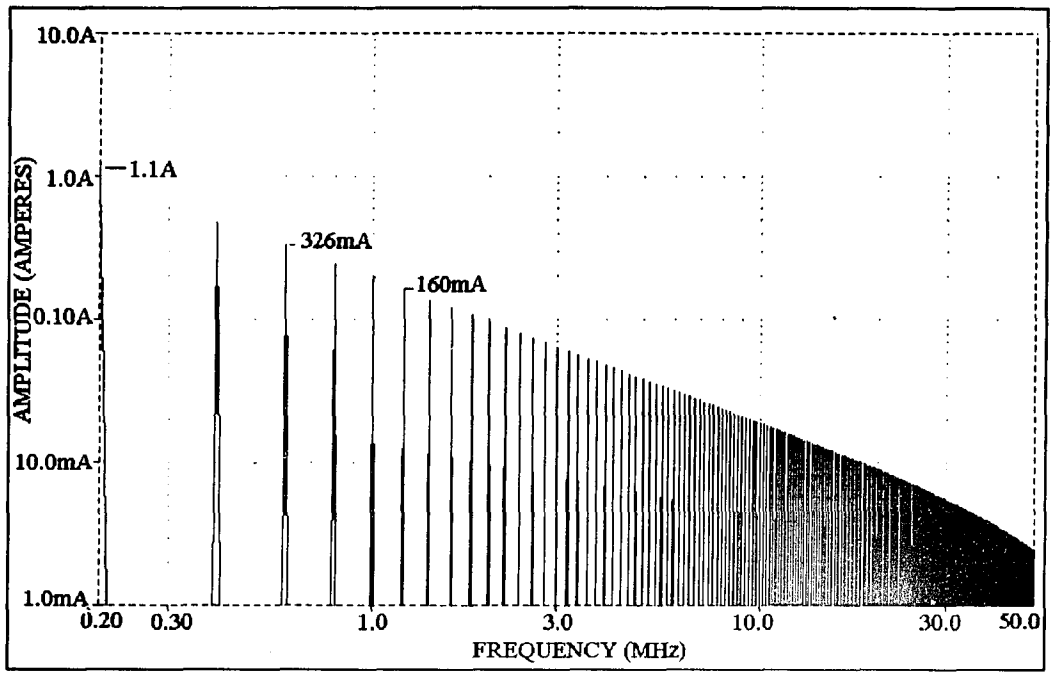

Figure 2.14-The harmonic spectrum of three identical waveforms combined with a phase shift of 0°.

Next the analysis is repeated with the waveforms evenly staggered across the switching period. This results in a phase shift of 120° between each waveform. The input current waveforms of the three converters and the combined current waveform are shown in Figure 2.15. The first converter switches on at 0 seconds, the second at one third of the switching period and the third at two thirds of the switching period. This evenly staggers the waveforms over the entire switching period as shown in the combined waveform at the bottom of Figure 2.15. The frequency spectrum of this combined waveform is shown in Figure 2.16.

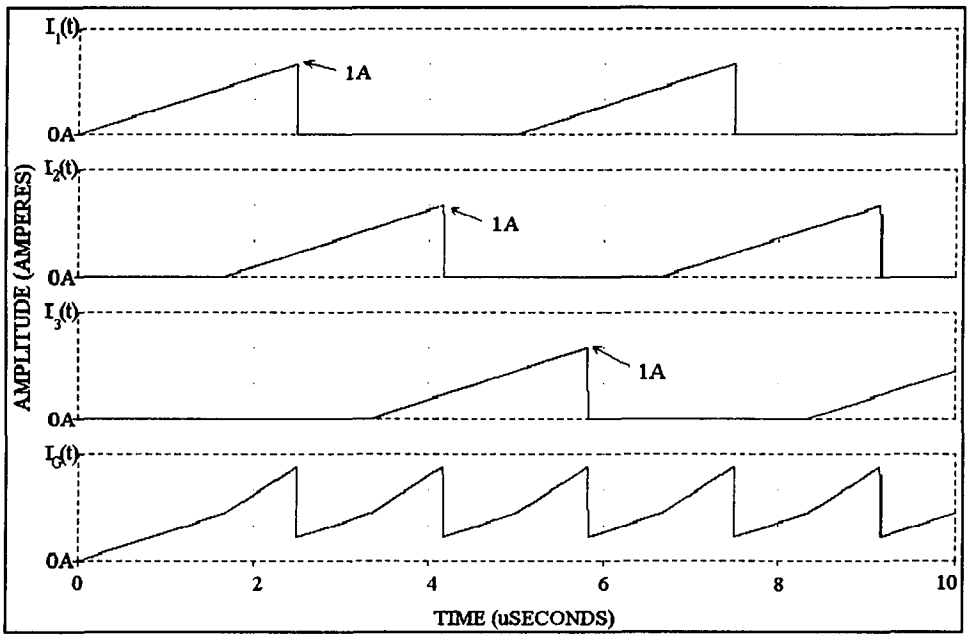

Figure 2.15-Three identical waveforms combined with a phase shift of 120°.

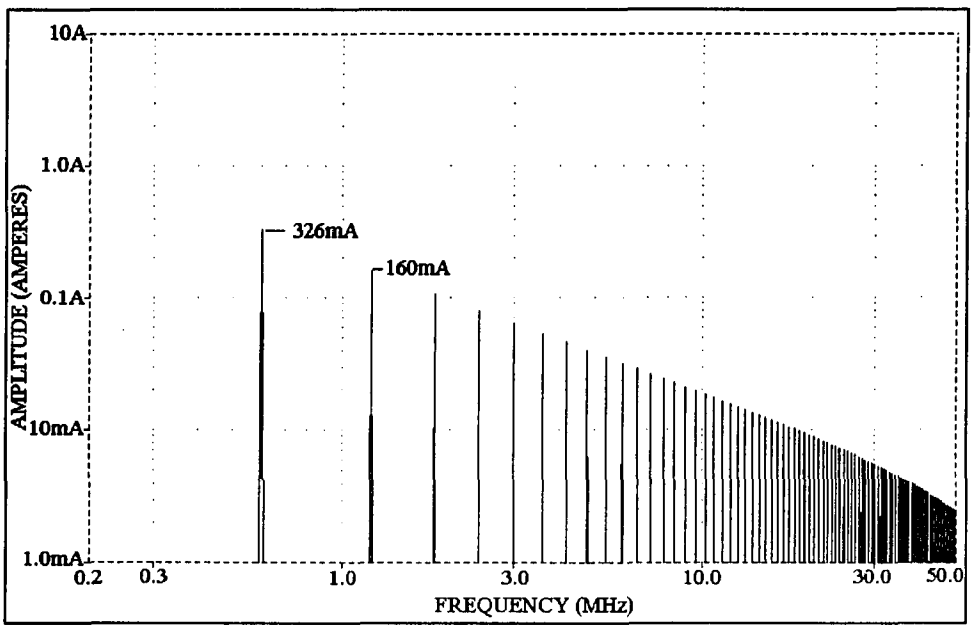

Figure 2.16-The frequency spectrum of the combined waveform of Figure 2.15

By evenly staggering the input current waveforms over the entire switching period the fundamental frequency is increased by a factor of three to 600kHz and two out of three harmonics are canceled. The harmonics that are not canceled have the same magnitude as in the case where the waveforms were combined with a phase shift of 0°. Another advantage is that the required EMI filter has an LC product one ninth the amount needed when the waveforms were combined with a phase shift of 0°.

2.5 The Optimal Phase Relationship For A System Of n Converters

The optimal phase relationship between converters with identical input current waveforms is a function of the number of converters in the system. In a system of n converters, the EMI filter requirements are minimized when the switching of each converter is controlled in such a way that a delay of 1/n of the switching period exists between each converter. In this way the combined waveform is uniformly distributed over the switching period, the amplitude of the sharply falling edge is minimized and n-1 out of n harmonic frequencies are canceled. The fundamental frequency is increased by a factor of n which results in a reduction of LC EMI filter product by $1/n^2$.

2.6 Effect Of Waveform Variations On System EMI

In the previous analysis, the input current waveforms generated by each of the DCM Flyback converters were assumed to be identical. In a real system, these waveforms will have variations in amplitude and duty cycle. The switching frequency does not vary significantly between converters because the circuitry that generates the switching frequency for the master converter can be used to control the switching frequencies of the other converters. But differences in the primary transformer inductance of each converter can result in significant variations between the peak amplitudes of the input current

waveforms. Also, when the load changes, the converter tries to regulate the output voltage by changing the duty cycle.

For a system of converters to have total cancellation of certain harmonics, the waveforms must have identical amplitudes and duty cycles and occur at intervals evenly spaced over the switching period of the combined waveform. If these parameters differ between waveforms, the combined frequency spectrum deviates from the ideal behavior discussed in the previous section. The effects of these variations can be determined mathematically by applying Equations 2.5 and 2.6 to each waveform, combining the coefficients a_n and b_n of each waveform and calculating the magnitude of each of the harmonics using Equation 2.8. The following sections investigate the impact that these variations have on the ability to reduce system EMI by combining the two waveforms with a phase shift of 180°.

2.6.1 EMI Due To Variations In Amplitude

In order to determine the effect that amplitude variations between converter waveforms has on the system EMI, a two converter system similar to the one shown in Figure 2.5 is analyzed. The two converters are assumed to be identical in every way except for a difference in the primary inductance values of the transformer. This difference can occur in a manufacturing environment where it is not always feasible to spend the time and money to ensure identical components. However, it can be controlled to be within a few percent of the nominal value. In this system, the primary inductance of each converter can be assumed to be within 10% of the nominal value.

In a previous section, it was shown that if these two converters have identical input current waveforms and are combined with a 180° difference in phase, then there is total

cancellation of odd harmonics in the combined waveform. The magnitude of these harmonics were given in Equation 2.18.

If, however, the two waveforms are combined with 180° phase shift and they have different peak amplitudes, A_1 and A_2, the odd harmonics will not totally cancel. This is shown mathematically in Equation 2.20. This equation shows how the amplitude variations between two waveforms effect the magnitude at each harmonic frequency and as expected, reduces to Equation 2.18 when A_1 equals A_2.

$$c_n = \sqrt{\left(\frac{2}{(n\pi)^2}\left[-A_1 + A_2\right]\right)^2 + \left(-\frac{1}{(n\pi)}\left[A_1 + A_2\right]\right)^2} \text{ if n is odd and,}$$

$$= \frac{1}{n\pi}\left[A_1 + A_2\right] \text{ if n is even} \qquad (2.20)$$

If the same two waveforms are combined with a phase shift of 0° the harmonic magnitude of the combined waveform is given by Equation 2.21 which reduces to Equation 2.13 when A_1 equals A_2.

$$c_n = \sqrt{\left(\frac{2}{(n\pi)^2}\left[A_1 + A_2\right]\right)^2 + \left(\frac{A_1 + A_2}{n\pi}\right)^2} \text{ if n is odd, and}$$

$$= \frac{A_1 + A_2}{n\pi} \text{ if n is even} \qquad (2.21)$$

As a numerical example, the following parameters are chosen for the converter shown in Figure 1.1 the turns ratio, n_1:n_2 is 1:1, the peak primary inductor current, I_G, is 1.0 Amperes, the duty cycle, D_1, is 50%, the switching frequency, f_S, is 200kHz. and the input voltage, V_G, is 28VDC. Substituting these values into Equation 1.22 the nominal value of the primary inductance was calculated to be 70μH. In this system one converter has the nominal primary inductance of 70uH and the other converter's primary inductance is allowed to change by 10% to 63uH. In this way the primary inductance between the

two converters differs by the maximum amount while one converter retains the nominal value. The resultant peak amplitudes are 1.1 and 1.0 Amperes respectively.

In the first case these two waveforms are combined with a 180° phase shift as shown in Figure 2.17. The combined waveform is then transformed into the frequency domain and is shown in Figure 2.18. It is apparent from Equation 2.20 as well as Figure 2.18 that the magnitude of the odd harmonic frequencies are no longer zero but are a function of the differences between the two peak amplitudes. The odd harmonics are still reduced in size, and can be effectively filtered by a filter designed to attenuate the even harmonics.

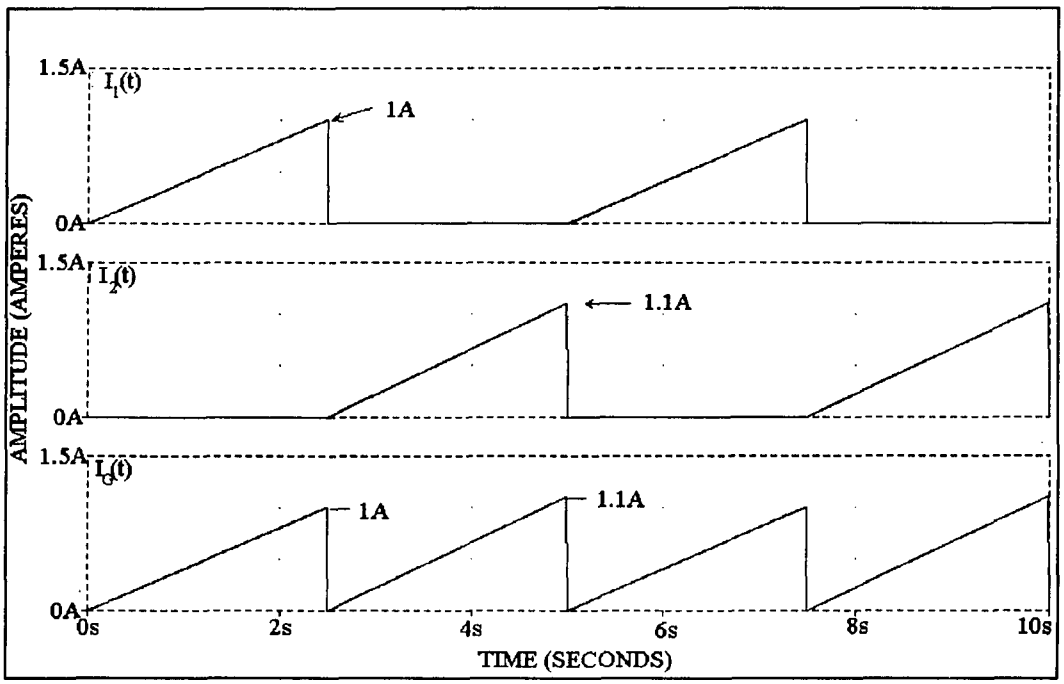

Figure 2.17-Two waveforms with different peak amplitudes are combined with a phase shift of 180°.

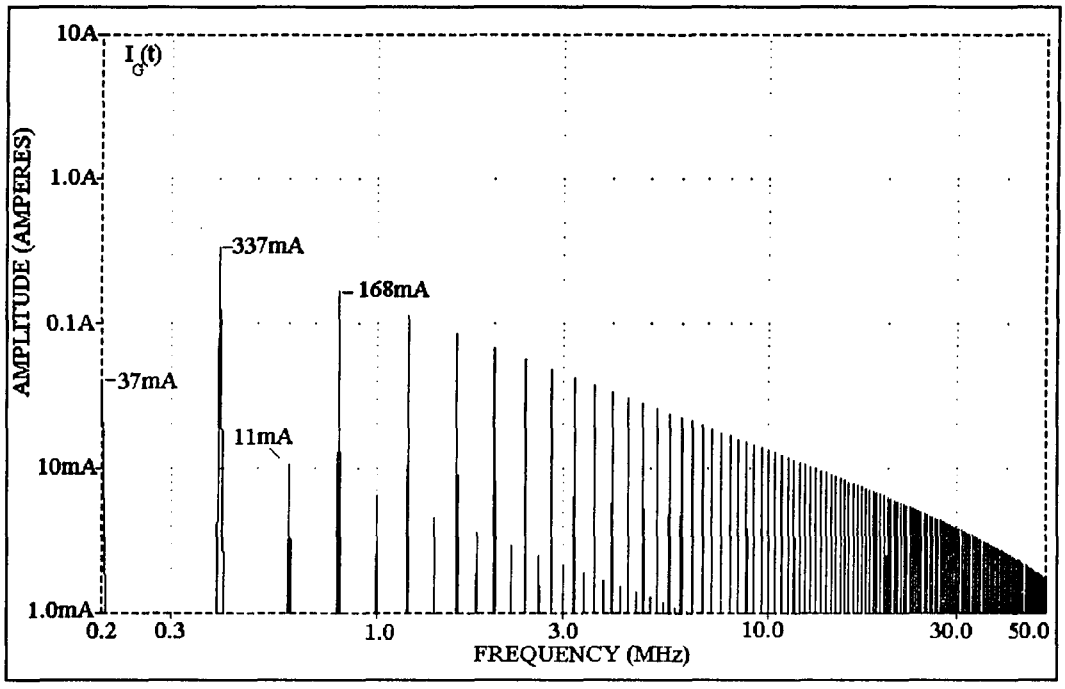

Figure 2.18-The frequency spectrum of the combined waveform, $I_G(t)$, of Figure 2.17

In order to compare this case to the case where the waveforms have a 0° phase shift, the two waveforms are combined with a phase shift of 0° as shown in Figure 2.19. The corresponding frequency components are show in Figure 2.20. Comparison of these two frequency spectra shows that the fundamental is 20dB lower when the waveforms are combined with a phase shift of 180° than for the case of a 0° phase shift, even though the odd harmonics did not completely cancel.

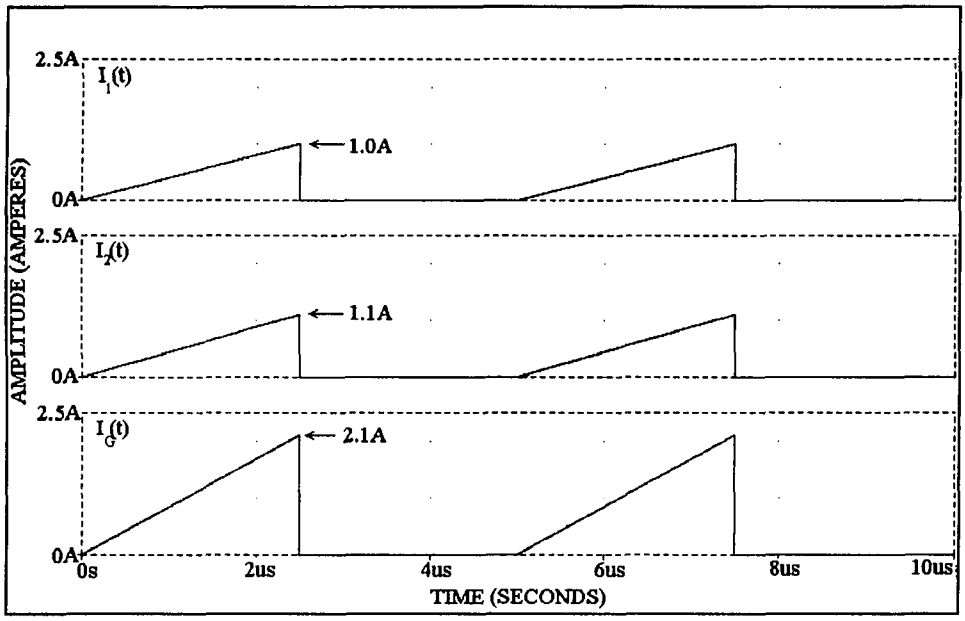

Figure 2.19-Two waveforms with different peak amplitudes are combined with a phase shift of 0°.

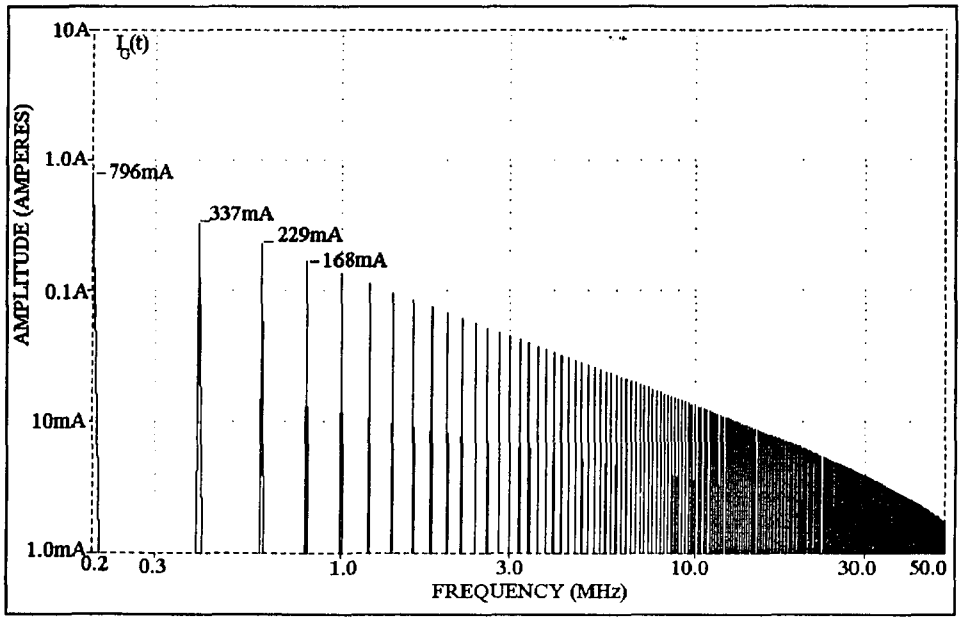

Figure 2.20-The frequency spectrum of the combined waveform, $I_G(t)$, of Figure 2.19

2.6.2 EMI Due To Variations In Duty Cycle

When different loads are applied to identical converters the duty cycles change and the input current waveforms are no longer identical. A two converter system similar to that shown in Figure 2.5 is used to determine if the amount of EMI in this case can still be reduced by combining the two waveforms with a phase shift of 180°.

In this case, the converters are assumed to be identical except they have different loads. The duty cycle of each converter is different as each converter regulates its own output voltage. The slope of the input current waveforms are the same but the peak amplitudes are different. The individual and combined waveforms are shown in Figure 2.20. The top waveform has a peak amplitude of 1.0 Ampere, a switching frequency of 200kHz. and a duty cycle of 50%. The middle waveform has the same switching frequency but since the duty cycle is 10% greater it has a peak amplitude of 1.1 Ampere. The bottom waveform, $I_G(t)$, is the result of the two waveforms combined with a phase shift of 0°.

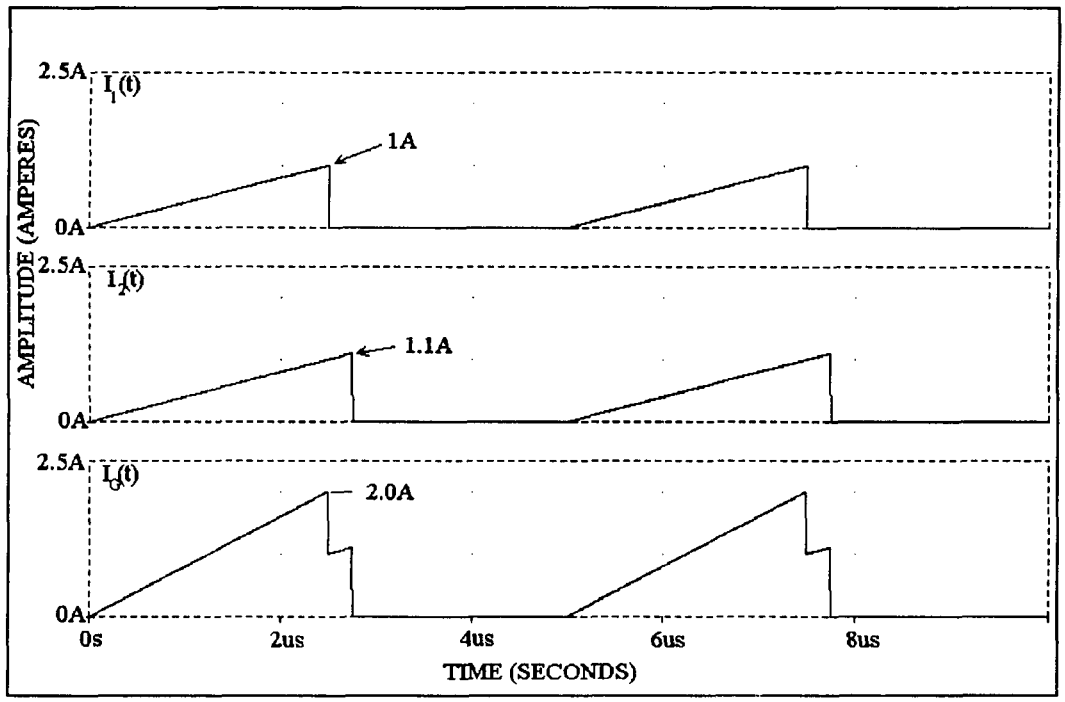

Figure 2.21-Two waveforms with different duty cycles are combined with a phase shift of 0°

The effects these variations have on the frequency content of the combined waveform can be derived symbolically using Equations 2.5-2.7 or graphically using PSPICE. Since the symbolic derivation is somewhat unwieldy, PSPICE is used to compare the frequency content of the two waveforms combined with a phase shift of 0° to the frequency content of the same two waveforms combined with a phase shift of 180°. The frequency content of the combined waveform, $I_G(t)$, of Figure 2.21 is shown in Figure 2.22.

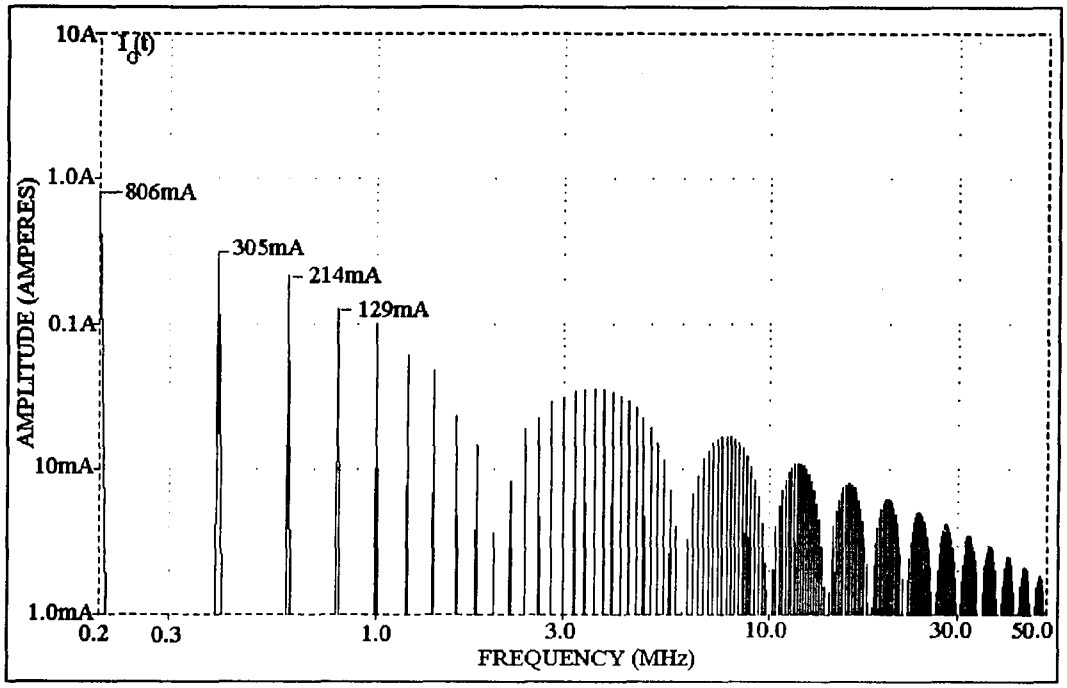

Figure 2.22-The frequency spectrum of the combined waveform, $I_G(t)$, of Figure 2.21

The same waveforms are combined with a phase shift of 180° as shown in Figure 2.23 and the frequency spectrum of the combined waveform is shown in Figure 2.24. Comparison of the two frequency spectrum shows that the magnitude of the fundamental frequency is reduced by 18dB, even though the odd harmonics did not completely cancel when the two waveforms where combined with phase shift of 180°.

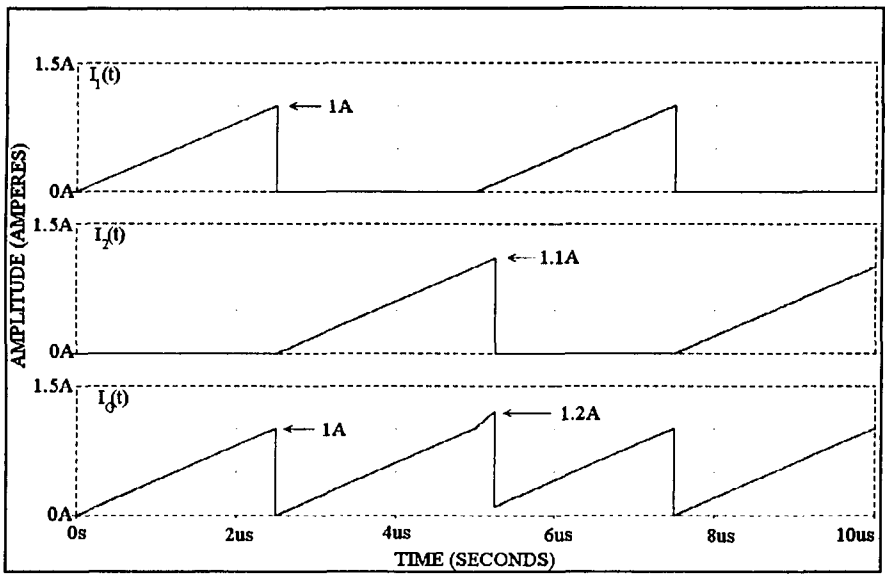

Figure 2.23-Two waveforms with different duty cycles are combined with a phase shift of 180°

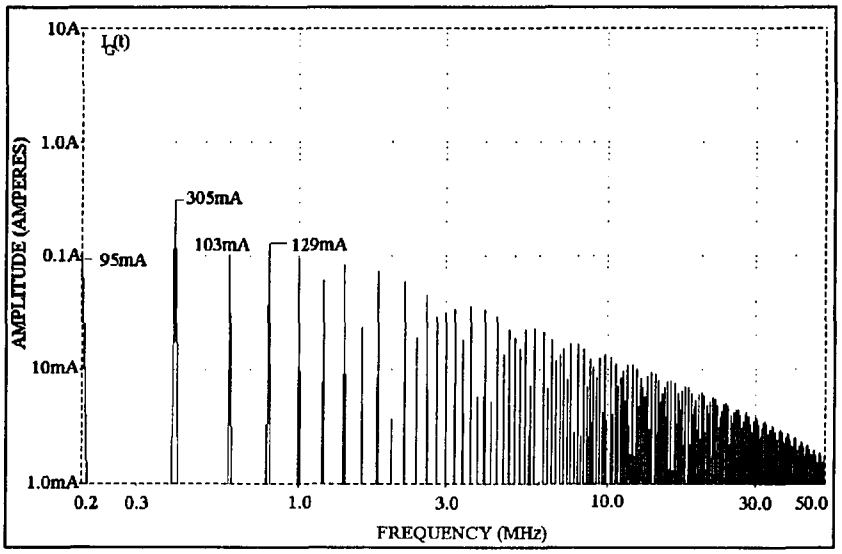

Figure 2.24-The frequency spectrum of the combined waveform, $I_G(t)$, of Figure 2.23

2.7 Reduction of RMS current

Another reason to combine 'n' triangular waveforms with a phase shift equal to 360°/n is to reduce the amount of RMS current in the combined waveform [7]. As an example, consider the two identical waveforms of Figure 2.8 which are combined with a phase shift of 0°. The RMS current of this combined waveform is 0.8165 A_{RMS}. This amount is derived from Equation 2.22 and Figure 2.8 where the duty cycle, D, is 0.5 and the peak amplitude, *Ipk*, is 2.0 Amperes. When the same waveforms are combined with a phase shift of 180°, as in Figure 2.10, the switching period of the combined waveform increases to 400kHz, the duty cycle, D, is now equal to 1.0 and the peak amplitude is 1 Ampere. The RMS value in this case is 0.5774 A_{RMS} which is 30% lower than the previous case.

$$Irms = Ipk\sqrt{\frac{1}{D}} \qquad (2.22)$$

Decreasing the amount of RMS current in the combined waveform reduces the power that is dissipated when the current flows through a resistive element. One type of resistive element that may be effected by the RMS current is the ESR associated with the low frequency shunt capacitor used in an EMI filter. If the ESR and the RMS current are large, the capacitor must be able to dissipate the power without adversely effecting the operation of the capacitor.

CHAPTER 3

DESIGN, SIMULATION AND MEASUREMENT OF A SYSTEM OF TWO DCM FLYBACK CONVERTERS AND EMI FILTER

3.0 Introduction

In the first part of this chapter a system of two parallel DCM Flyback converters with similar switching frequencies is designed and constructed. This system is capable of combining the input current waveforms, $I_G(t)$, generated by each converter with a phase shift of 0° or 180° on the voltage bus. The input current waveforms generated by each converter is measured on an oscilloscope and the EMI of the combined waveform is measured on a spectrum analyzer for each of the phase relationships. The system operation is then simulated using PSPICE. The measured input current waveforms are modeled as ideal triangular waveforms and are combined with a phase shift of either 0° or 180°. The amount of simulated EMI is measured for each case. These simulated measurements are then compared to the experimental measurements to show how accurately the ideal triangular waveform models the true input current waveform generated by a DCM Flyback converter. This experiment also shows that the conducted EMI on the voltage bus can be substantially reduced if the two input current waveforms have a phase difference of 180°.

Even though there is a substantial reduction in the amount of EMI when the two converters are 180° out of phase, the system EMI in both cases exceeds acceptable limits. The second part of this chapter contains the design, simulation and construction of the EMI filters required for each case. The design illustrates the benefit of combining the two waveforms with a phase shift of 180°. By combining the two input current waveforms in such a way, the magnitude of the fundamental frequency and all odd harmonics of the combined waveform are significantly reduced. This effectively doubles the fundamental

frequency of the combined waveform. Since the EMI filter is designed to provide sufficient attenuation at the fundamental frequency, which is now twice the frequency as when the waveforms are combined with a phase shift of 0°, the required amount of EMI filter is theoretically reduced by a factor of four. An EMI filter is first designed for the case where the input current waveforms are combined with a phase shift of 0°. The actual filter, including measured parasitic elements is simulated using PSPICE. This simulated filter is used to filter the simulated combined input waveforms and the simulated EMI is reduced to the desired level. This filter is then constructed and used to filter the combined input current generated by the converters. The amount of EMI is then measured using the spectrum analyzer and found to be very close to the simulated value.

The last part of this chapter contains a filter design for the case where the two input current waveforms are combined with a phase shift of 180°. The reduction of the EMI filter by one fourth is incorporated by reducing the value of the low frequency inductor by a factor of four while keeping all other parameters constant. This filter and the combined input current waveform is also simulated and the amount of the EMI of the simulated filtered waveform measured. This filter is then constructed and used to filter the combined input current generated by the converters. The amount of EMI is measured and compared to the simulated EMI value. In both cases, the measured values are very close to the simulated values.

3.1 System of Two DCM Flyback Converters

The system shown in Figure 3.1 is used to illustrate the advantages of combining triangular waveforms in such a way that the resulting peak amplitude is minimized. This reduces the amount of both the conducted EMI and the RMS current that is seen on the voltage bus. The advantages are the ability to use a smaller EMI filter and components with lower power ratings.

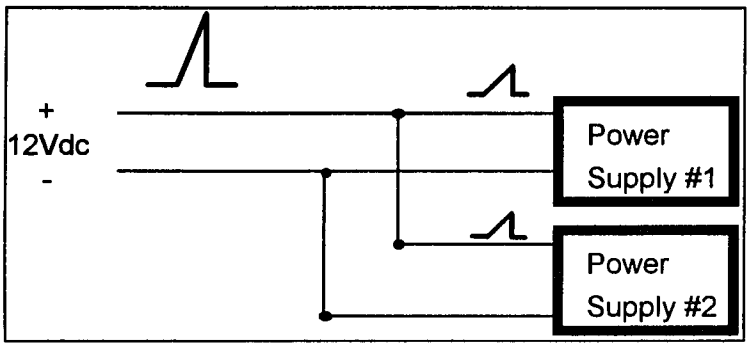

Figure 3.1-System of Two SMPS

For simplicity, this system contains only two switched mode power supplies (SMPS) connected in parallel on the DC voltage bus. These power supplies are DCM Flyback converters with triangular input current waveforms that are characteristic of all SMPS. The particular way that the individual waveforms combine on the voltage bus depends upon the phase relationship between the gate drivers of each MOSFET. It is the frequency content of this combined waveform that determines the amount of EMI that will appear on the dc voltage bus.

It has been previously shown that if two identical triangular waveforms are combined with a phase shift of 180° both the conducted EMI and the RMS current on the voltage bus can be minimized. Since it is impossible to construct and operate two converters with identical input current waveforms, an attempt was made to minimize the differences. This was achieved by designing two identical converters that supply power to constant loads. In this way the only differences between the individual waveforms are due to variations between individual components.

3.2 System Design

The schematic diagram of the system is shown in Figure 3.2. A pulse width modulator (PWM) is used in each converter to control the switching frequency and regulate the output voltage. The PWM used in this application is the Unitrode 1846

current mode PWM controller. This PWM has synchronization capabilities and dual output gate drivers that are phase shifted by 180°. These features are used to synchronize the two converters and provide both 0° and 180° phase shift between the two input current waveforms.

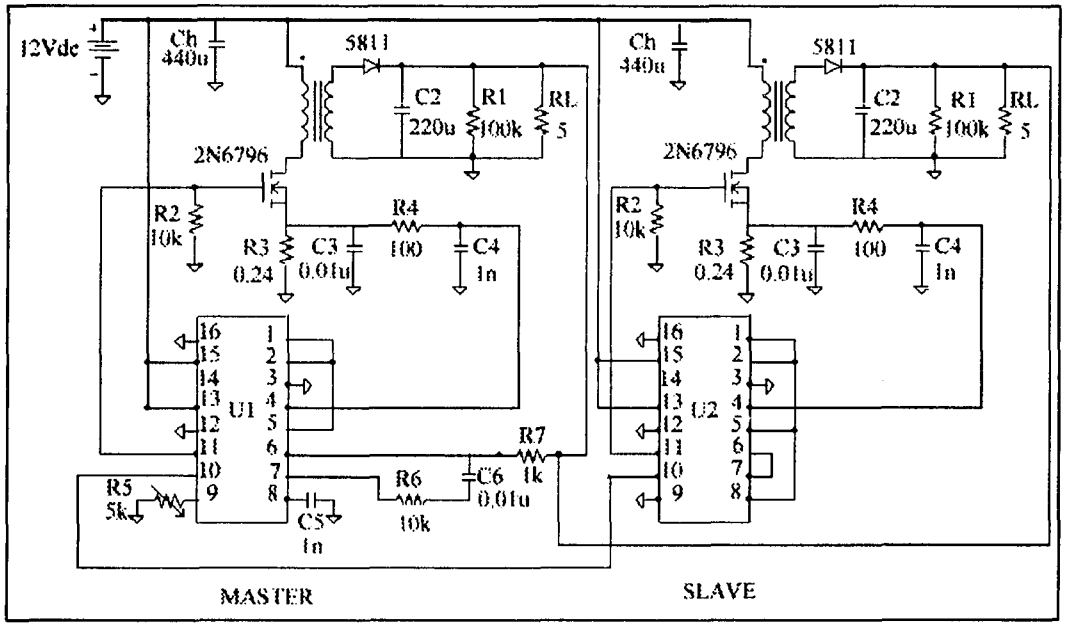

Figure 3.2-System Schematic Diagram

The converter design procedure is similar to that described in Chapter 1 with V_G=12Vdc, V_O=5Vdc, R_L=5Ω, D_1=0.45 and the peak value of $I_G(t)$=2.5 Amperes. The resulting primary and secondary inductance of the transformers are 8μH and 5μH respectively. The transformers were designed using a series 1408 pot core with an A_L of 100 and AWG 28 insulated wire. The 2N6796's are N-Channel Enhancement-Mode Power Field-Effect Transistors and the diodes are 1N5811.

If the load of the converter is removed, the output voltage can exceed safe operating levels. This can be seen from Equation 1.21 as R_L goes to infinity. To prevent this, a

100kΩ resistor, R_1, is connected across the output of each converter. In order to provide hold up capability [7], four 110μF electrolytic capacitors were connected between the voltage bus and ground on each converter. Two 110μF and two 1μF capacitors are also connected across the output of each converter to limit the amount of voltage ripple.

The converter on the left side of Figure 3.2 is the *master* and the one on the right is the *slave*. In this configuration the 200kHz switching frequency of the *master* converter is set by C_5 and R_5 which in turn sets the switching frequency of the *slave* converter. If this PWM had a single gate drive, this configuration would insure that the two converters were always in phase with each other. However, since this PWM has two gate drivers that have a phase difference of 180°, it is possible that the two converters will have a phase difference of either 0° or 180°. This depends on how the *master* synchronization pulse triggers the gate drivers of the *slave* PWM at turn on. By connecting the gate of each MOSFET to the same output driver on each PWM, the two input current waveforms will be combined with either a 0°or 180° phase shift simply by resetting the bus voltage until the desired condition is obtained. The frequency content of this combined waveform can then be measured using a spectrum analyzer for both of the phase relationships.

3.3 System Construction and Measurement of EMI

The system of Figure 3.2 was constructed on a "vector" board with one side coated with copper. The components were connected at isolated points and the ground plane was kept as large and as continuous as possible. This type of "vector" board used in this manner provides an excellent ground plane that minimizes noise problems. The voltage bus is supplied by an external 12V dc power supply. When power was applied to the system the converters regulated the outputs at 5Vdc and the input current waveforms, $I_G(t)$, generated by each converter could be measured by a current probe.

In order to compare the two waveforms it was necessary to apply a fixed load to each converter. A 10Ω load was selected and applied to the output of each converter. The waveforms were then measured individually using a current probe around the primary transformer wire where it is connected to the voltage bus. A plot containing the MOSFET gate voltage and $I_G(t)$ generated by the *master* converter is shown in Figure 3.3. The top waveform is the gate voltage measured at 10Volt/Division and the bottom waveform is $I_G(t)$ measured at 1Ampere/Div. The current waveform has a frequency of 200kHz with a peak amplitude of 2.4 Amperes and a duty cycle of 0.32 with the 10Ω load.

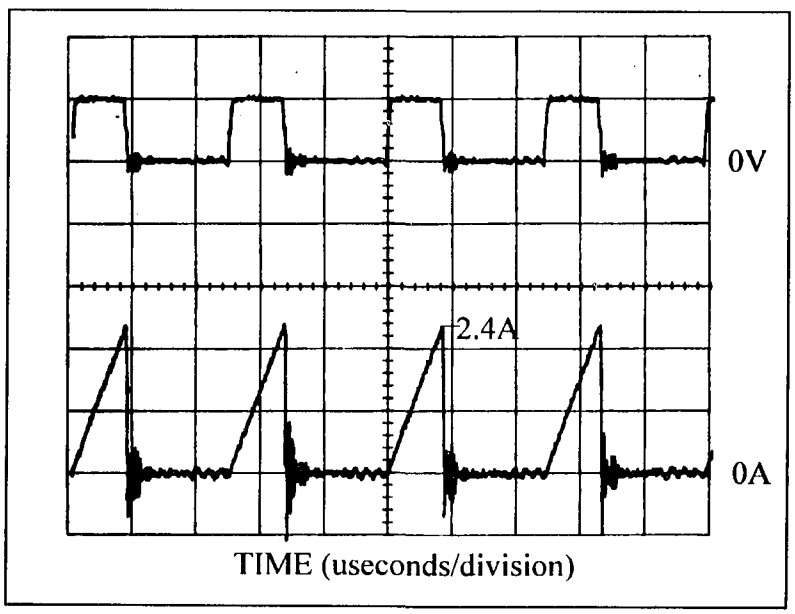

Figure3.3-Master Converter's Gate Voltage (top- 10V/div) and Input Current (bottom) Waveforms Measured on Oscilloscope

The input current generated by the *slave* converter is identical to this waveform with the exception that the peak amplitude is 2.2 Amperes. This difference is due to transformer variations between the two converters.

The combined waveform is also measured using the current probe at the voltage bus. When the two converters are in phase with each other the waveforms combine as shown in Figure 3.4. The top waveform is the *Master* gate voltage with 10Volts/division and the bottom waveform is the *slave* $I_G(t)$ with 1Ampere/division. Note that the switching frequency and the duty cycle remained the same but the peak amplitude is now the sum of the individual peak amplitudes.

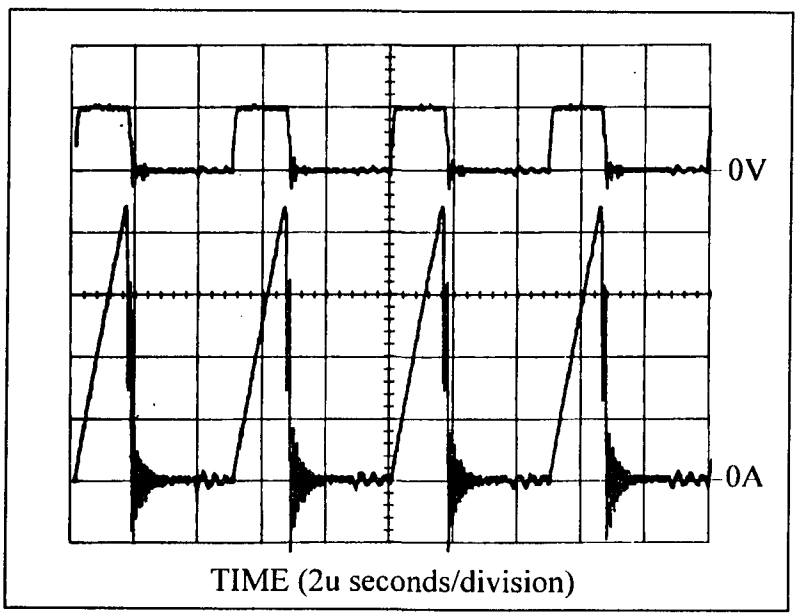

Figure3.4-Master Converter's Gate Voltage (top- 10V/div) and 0° Combined Input Currents (bottom-1A/div) Waveforms Measured on Oscilloscope

The frequency content of the combined waveform is measured with a spectrum analyzer as shown in Figure 3.5. The y-axis is logrithmic magnitude in units of dBm with grid spacing of 10dBm/division. The x-axis is a linear scale of frequency in units of Hertz with grid spacing of 200kHz/division. The frequency range is from 100kHz to 2MHz which shows the magnitude of the first ten harmonics. The magnitude at 200kHz is

measured as 23dBm which converts to 121dBμA by taking into account the current probe factor at 200kHz.

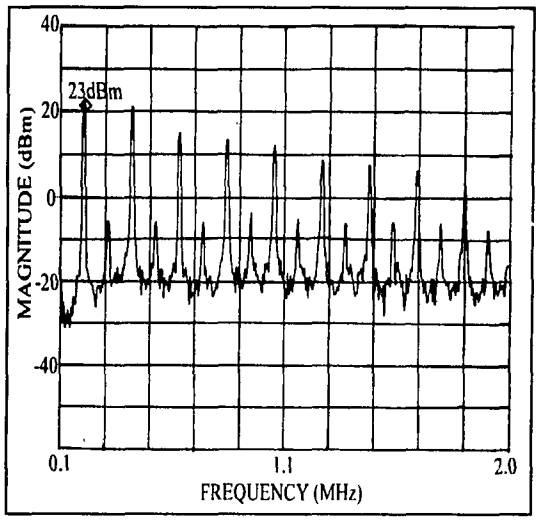

Figure 3.5-Frequency Spectrum of the Combined Waveform of Figure 3.4

These measurements are repeated with the converters input current waveforms combined with a phase difference of 180°. This condition is obtained by switching the bus voltage off and on at the external power supply until the control chips inverted their output signals so the waveforms combined with a phase shift of 180°. All other system parameters remained the same. The combined waveform is shown in Figure 3.6. The harmonic content of this waveform measured on the spectrum analyzer is shown in Figure 3.7. Here the magnitude at 200kHz is 0.96dBm or 99dBμA which is approximately 22dB lower than it was for the case where the waveforms were combined with a phase shift of 0°. Also worth noting is the fact that the magnitude of the even harmonics remain the same in both cases but the magnitudes of the odd harmonics are consistently lower in the case where the two waveforms are 180° out of phase.

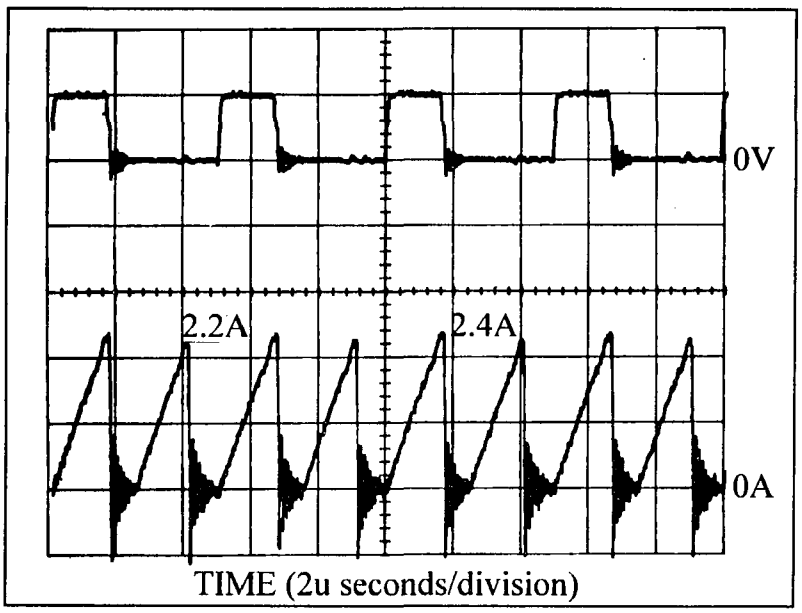

Figure3.6-Master Converter's Gate Voltage (top- 10V/div) and 180° Combined Input Currents (bottom-1A/div) Waveforms Measured on Oscilloscope

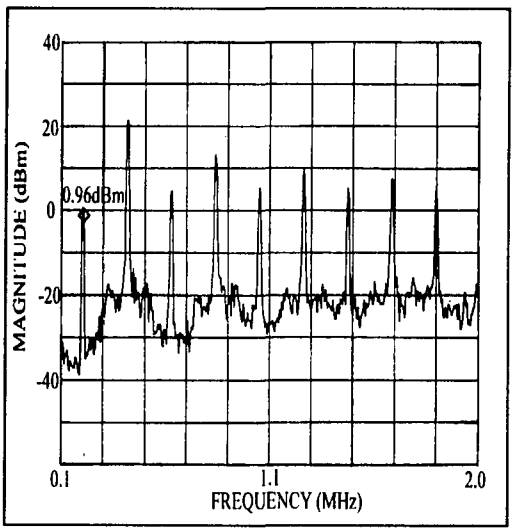

Figure 3.7-Frequency Spectrum of the Combined Waveform of Figure 3.6

3.4 EMI filter Design, Construction and Measurement

Although there is a significant reduction in the magnitude of the fundamental frequencies between the two cases, the frequency spectrum for both cases still exceeds the EMI limit described in Figure 1.7. The harmonic magnitudes at the fundamental frequency are approximately 49dB and 71dB over the limit when the two waveforms are combined with 180° and 0° phase shift, respectively.

As mentioned earlier, if two identical triangular waveforms are combined with a phase shift of 180°, the fundamental frequencies and all the odd harmonics would cancel. This effectively moves the fundamental frequency from 200kHz to 400kHz and the required EMI filter could have a low frequency LC product one fourth the size of the product needed for the case where the two waveforms are combined at 0°. Although the waveforms are not identical, they are similar enough for this theory to work. This will be shown in the following sections where two EMI filters will be designed and constructed. The first one will be designed for the 'worst' case when the waveforms are combined with a 0° phase shift and the second for the case when the waveforms are combined with a 180° phase shift. The only parameter that will change between the two filters in the value of the low frequency inductor. The low frequency inductance needed for the worst case filter will be four times the inductance needed for the other filter.

3.4.1 EMI Filter Design-Converters in Phase

The EMI filter was first designed for the case where the two waveforms are combined with a phase shift of 0°. This filter must be able to reduce the frequency content of Figure 3.5 by 71dB at 200kHz. In order to simulate the effectiveness of the filter during the design process, the unfiltered combined waveform of Figure 3.4 was modeled as an ideal triangular waveform using PSPICE. The frequency spectrum of this waveform was also generated using PSPICE and is shown in Figure 3.8.

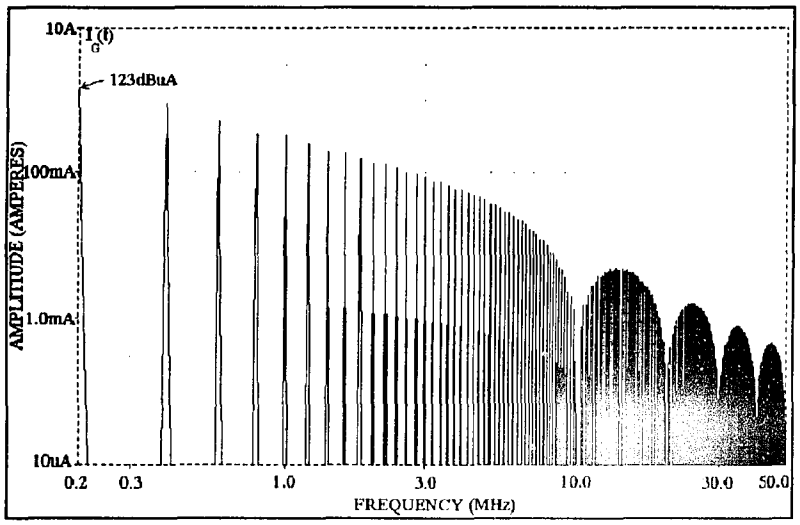

Figure 3.8-Simulated Frequency Spectrum of Waveforms Combined with 0° Phase Shift

The magnitude of the fundamental frequency of this simulated waveform is 123dBμA. This value is very close to the 121dBμA that was measured using the spectrum analyzer. Now that a model for the unfiltered waveform has been generated, the next step is to model the filter.

The ideal filter:

The EMI filter design procedure is similar to that discribed in Chapter 1.4. The ideal filter for this application is shown in Figure 3.9, where $I_G(t)$ and $I_B(t)$ are the unfiltered and filtered input current waveforms generated by the two DCM Flyback converters. The filter attenuation is shown mathematically in Equation 3.1. The attenuation is derived graphically using Equation 3.1 and the Method of Asymptotes [7] and the result is shown in Figure 3.10. This 'ideal' filter has infinite Q at the corner frequencies F_L and F_H. The mathematical expressions for these frequencies are shown in Equations 3.2 and 3.3. The attenuation of this filter at 200kHz is 120dB which is 48dB over the required attenuation

of 72dB. This margin should allow for the non ideal component parameters that are inherent to the filter components.

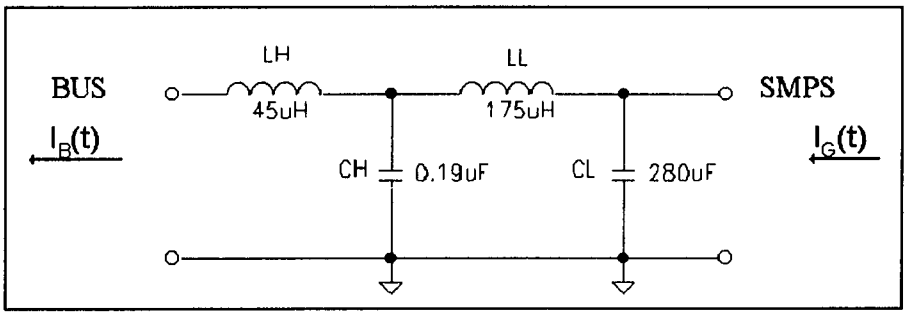

Figure 3.9-EMI Filter with ideal elements

$$H(s)\frac{I_b(s)}{I_g(s)} = \left(\frac{\frac{1}{sC_H}}{\frac{1}{sC_H}+sL_H}\right)\bullet\left(\frac{\frac{1}{sC_L}}{\frac{1}{sC_L}+sL_L+\left(sL_H \left\| \frac{1}{sC_H}\right.\right)}\right) \qquad (3.1)$$

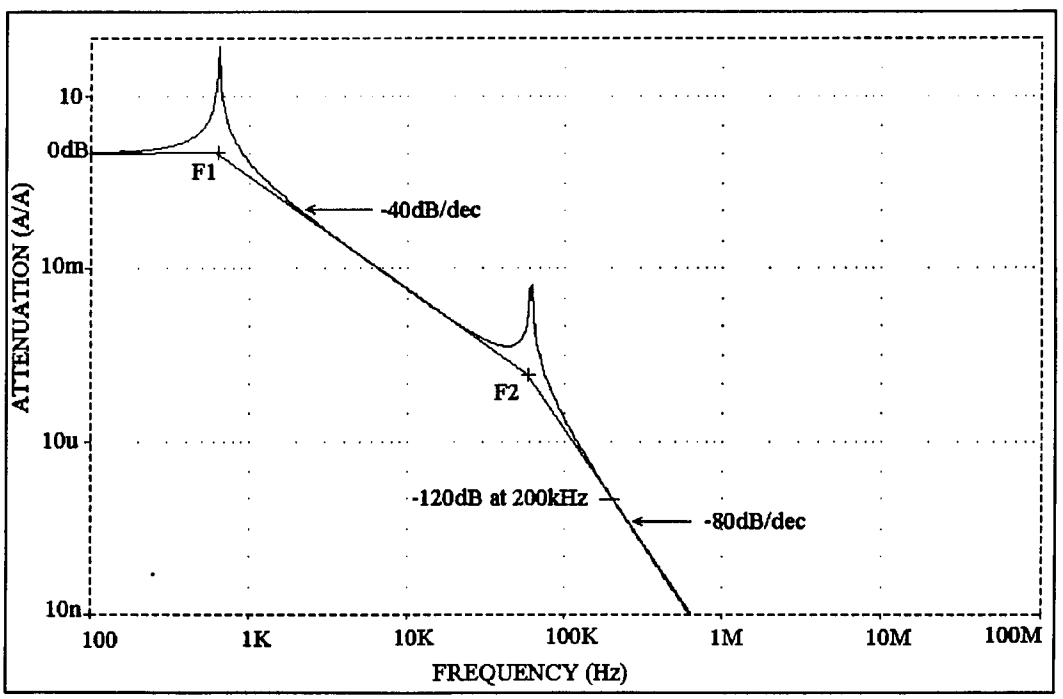

Figure 3.10-Current Attenuation of Filter of Figure 3.9

$$F_L = \frac{1}{2\pi\sqrt{L_L C_L}} = 719\ Hz \tag{3.2}$$

$$F_H = \frac{1}{2\pi\sqrt{L_H C_H}} = 54\ KHz \tag{3.3}$$

The filter with parasitic elements:

As mentioned earlier, components such as capacitors and inductors are not ideal. Their behavior changes over frequency. This non ideal behavior is caused by parasitic elements that are due to the physical construction of the components. In order to correctly model the filter, these parasitic elements must be included.

The parasitic elements of the main filter components were measured using a network analyzer. These parasitics are added to the ideal filter model as shown in Figure 3.11. Also included at this time are the parasitics, L_B and R_B, that are inherent to the voltage Bus. The attenuation of this filter is shown mathematically in Equation 3.4 and is derived graphically using the Method of Asymptotes [7] in Figure 3.12. The mathematical expressions relating each corner frequency to the filter elements are shown in Equations 3.5-3.13.

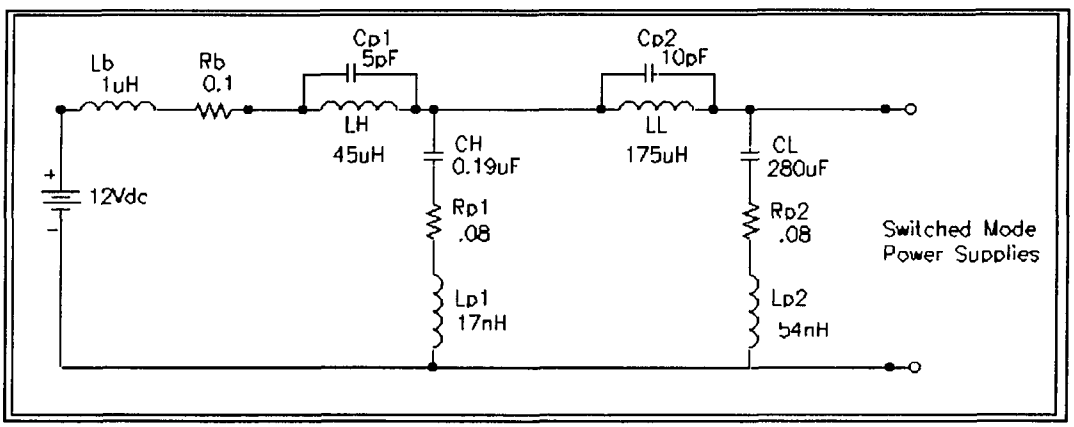

Figure 3.11-The Filter with Parasitic Elements

$$\frac{I_B(s)}{I_G(s)} = \left(\frac{\frac{1}{sC_H} + R_{P1} + sL_{P1}}{\left(\frac{1}{sC_H} + R_{P1} + sL_{P1}\right) + \left(\frac{1}{sC_{P1}} \| sL_H\right) + (sL_B + R_B)} \right) \bullet \left| \left(\frac{\left(\frac{1}{sC_L} + R_{P2} + sL_{P2}\right)}{\left(\frac{1}{sC_L} + R_{P2} + sL_{P2}\right) + \left(\frac{1}{sC_{P2}} \| sL_L\right) + \cdots \left(\left(\frac{1}{sC_{P1}} \| sL_H\right) + sL_B + R_B\right) \| \left(\frac{1}{sC_H} + R_{P1} + sL_{P1}\right)} \right) \right| \tag{3.4}$$

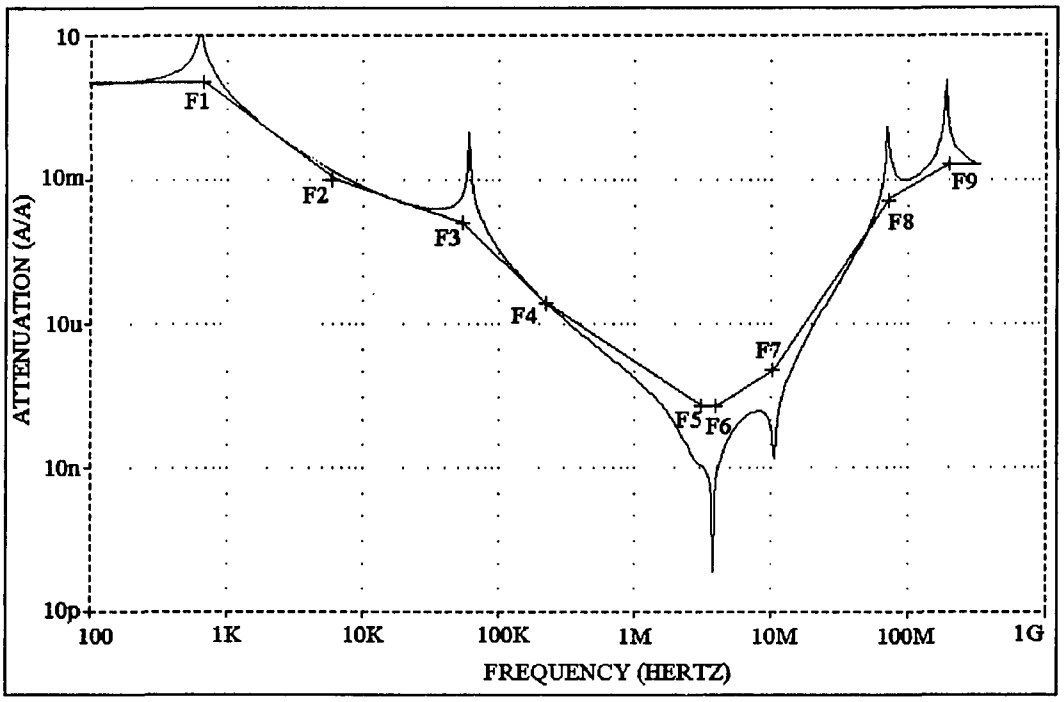

Figure 3.12-Filter Attenuation Showing the Effects of the Parasitic Elements

$$F_1 = \frac{1}{(2\pi)\sqrt{C_L L_L}} = 718\ Hz \tag{3.5}$$

$$F_2 = \frac{1}{(2\pi)R_{P2}C_L} = 7.1\,KHz \tag{3.6}$$

$$F_3 = \frac{1}{(2\pi)\sqrt{C_H L_H}} = 54\,KHz \tag{3.7}$$

$$F_4 = \frac{R_{P2}}{(2\pi)L_{P2}} = 237\,KHz \tag{3.8}$$

$$F_5 = \frac{1}{(2\pi)\sqrt{C_H L_{P1}}} = 2.8\,MHz \tag{3.9}$$

$$F_6 = \frac{1}{(2\pi)\sqrt{L_L C_{P2}}} = 3.8\,MHz \tag{3.10}$$

$$F_7 = \frac{1}{(2\pi)\sqrt{L_H C_{P1}}} = 10.6\,MHz \tag{3.11}$$

$$F_8 = \frac{1}{(2\pi)\sqrt{L_B C_{P1}}} = 71\,MHz \tag{3.12}$$

$$F_9 = \frac{1}{(2\pi)\sqrt{C_{P2} L_{P2}}} = 217\,MHz \tag{3.13}$$

The filter with damping components:

In order to simulate how well the filter attenuates the unfiltered waveform of Figure 3.4, all resonant points must be sufficiently damped. This is necessary to insure that PSPICE converges in a timely manner. It is also desirable to dampen any resonance points that occur at or below the power supply switching frequency. This will prevent stability problems within the feedback loops that regulates the power supplies.

There are three resonant points that must be damped in order to simulate the filter operation using PSPICE. The first one at 720Hz is caused by L_L and C_L, the second at 54kHz is due to L_H and C_H and the third one at 71MHz is caused by L_{BUS} and the parasitic

capacitance of L_H. These resonant points are damped using a series capacitor and resistor network that is added as shunt elements to the filter as shown in Figure 3.13. C_{D1} and R_{D1} are used to damp the resonance between L_{BUS} and C_{PLH}. C_{D2} and R_{D2} are used to damp the resonance between L_H and C_H and C_{D3} and R_{D3} are the damping elements for the resonance between L_L and C_L. The values of the damping capacitors are chosen to be approximately ten times the value of the capacitor that is being damped. The values of the damping resistors are determined by the characteristic impedance of the resonant elements, $R_D=(L/C)^{1/2}$.

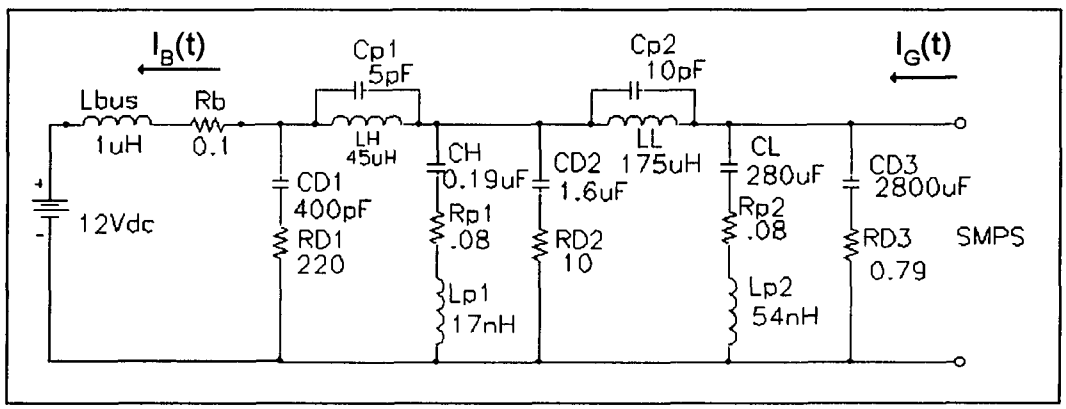

Figure 3.13-EMI Filter with Parasitic and Damping Elements

The current attenuation of the simulated filter with damping and parasitic elements is shown in Figure 3.14. This figure shows the adverse effect that the parasitic elements have on the attenuation of the filter. The filter can still properly attenuate the input current waveform even though the attenuation has decreased from 120dB to 91dB at 200kHz.

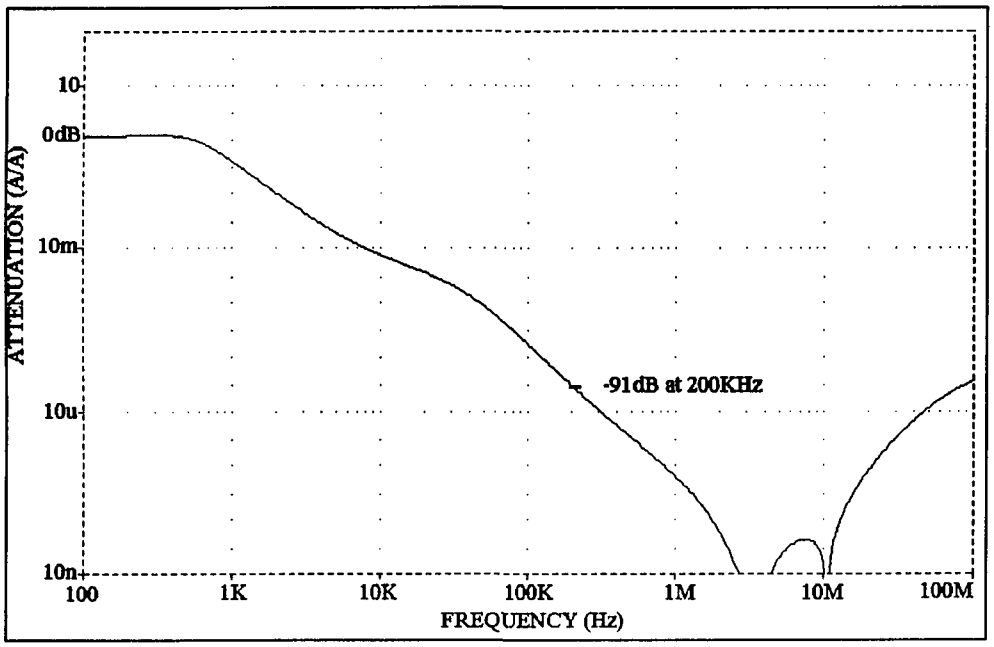

Figure 3.14-Current Attenuation of Filter with Parasitic and Damping Elements

The ability of the filter to attenuate the input waveform is demonstrated using PSPICE. The resulting frequency spectrum of the filtered waveform is shown in Figure 3.15. The magnitude of the fundamental frequency is 35dBμA which is well below the 50dBμA EMI limit at that frequency.

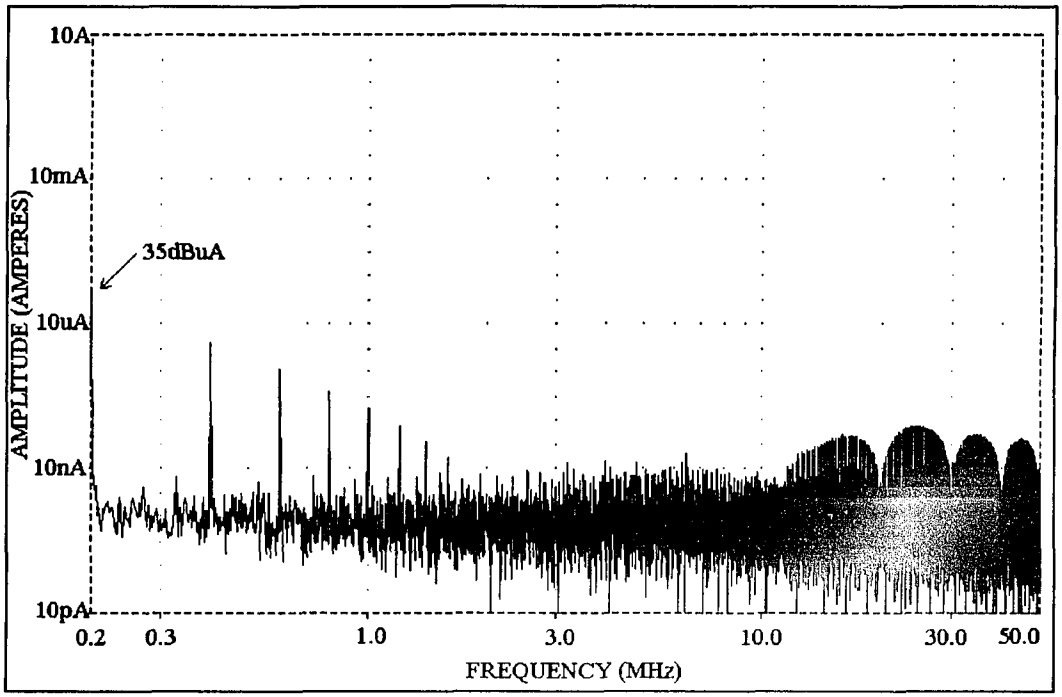

Figure 3.15-Simulated Frequency Spectrum of the Filtered Output when the Waveforms are Combined with a 0° Phase Shift

The construction and measurement of the filter:

The filter was constructed on a separate "vector" board. This vector board also had one side coated with copper to provide a good ground plane. The power supply board and the filter board were attached on one side by short jumper wires soldered to the ground planes every 1/4 inch. This provides a good ground plane between the power supplies and the filter. The inductors were placed away from the power supply transformers and fairly far apart from each other to prevent coupling, the extra length in these series elements will not reduce the efficiency of the filter. If anything it will add a few tenths of a nH to the inductance. On the other hand, the lead length on the capacitors

are kept to a minimum since any additional amount of lead inductance in the shunt elements of the filter could reduce the efficiency of the filter.

The two "hold-up" capacitors, C_H, connected to the voltage bus at each converter input were removed at this time to prevent them from adding to the low frequency filtering capacitor, C_L. The 2,800μF damping capacitor, C_{D3}, and the damping resistor, R_{D3}, are not included in the actual filter design because of the size and cost of such a capacitor. This damping network was included in the PSPICE analysis primarily to ensure that PSPICE converged in a timely matter. If stability problems arise due to this resonant point, this damping network or another more suitable damping network can be added to the filter. For convenience in constructing the filter the two remaining damping networks are connected to isolated points on the ground side of the board.

After power is applied to the system, the phase relationship between the two input current waveforms is verified to be 0°. The filtered waveform is measured with the spectrum analyzer as shown Figure 3.16 where the y-axis is logrithmic magnitude measured in 10dBm/division and the x-axis is frequency in 200kHz/division. The magnitude at 200kHz is -75.1dBm which is well below the limit of -48dBm at that frequency. The filter attenuated the input current by 98dB which is very close to the simulated filter attenuation of 91dB at 200kHz. The extra 7dB of attenuation is probably due to a discrepancy in measuring the parasitic elements of the filter elements.

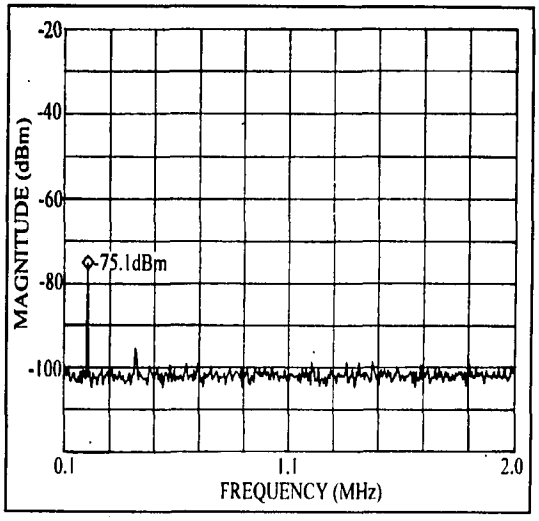

Figure 3.16-Filtered Frequency Spectrum of the Input Current Waveform Shown in Figure 3.4

3.4.2 EMI Filter Design-Converters 180° out of Phase

When the two input current waveforms combine with a phase shift of 180° as shown in Figure 3.6, the resultant frequency spectrum was measured as shown in Figure 3.7. Since the EMI limit is -48dBm at 200kHz, the filter must provide at least 49dB attenuation at this frequency.

The goal of the filter is to provide sufficient attenuation at the fundamental frequency, in this case 200kHz. If the two waveforms are identical and they are combined with a phase shift of 180°, the fundamental frequency and all the odd harmonics would cancel. This causes the fundamental frequency of the combined waveform to shift from 200kHz to 400kHz. The filter can then be designed for the higher frequency with the low frequency filter components, L_L and C_L, having an LC product one fourth the value needed to filter the waveforms combined with a 0° phase shift.

Even though the two waveforms are not identical, when they combine with an 180° phase shift the harmonic magnitude at 200kHz is decreased by 22dB. This can be seen by

comparing the measured frequency spectra of Figure 3.5 to Figure 3.7. This partial cancellation in the fundamental frequency naturally leads to investigating a filter design that uses an LC product one fourth the value used in the previous filter.

Filter Design:

In order to simulate the effectiveness of this filter during the design procedure, the combined input waveform of Figure 3.6 was modeled using PSPICE. The simulated frequency spectrum of this unfiltered waveform is shown in Figure 3.17. Comparing this simulated frequency spectrum to that measured in Figure 3.7 shows very good correlation between simulated results and actual measured values. At 200kHz the simulated magnitude is 96dBμA and the measured value converts to 99dBμA at 400kHz the simulated magnitude is 120dBμA and the measured value converts to 119dBμA.

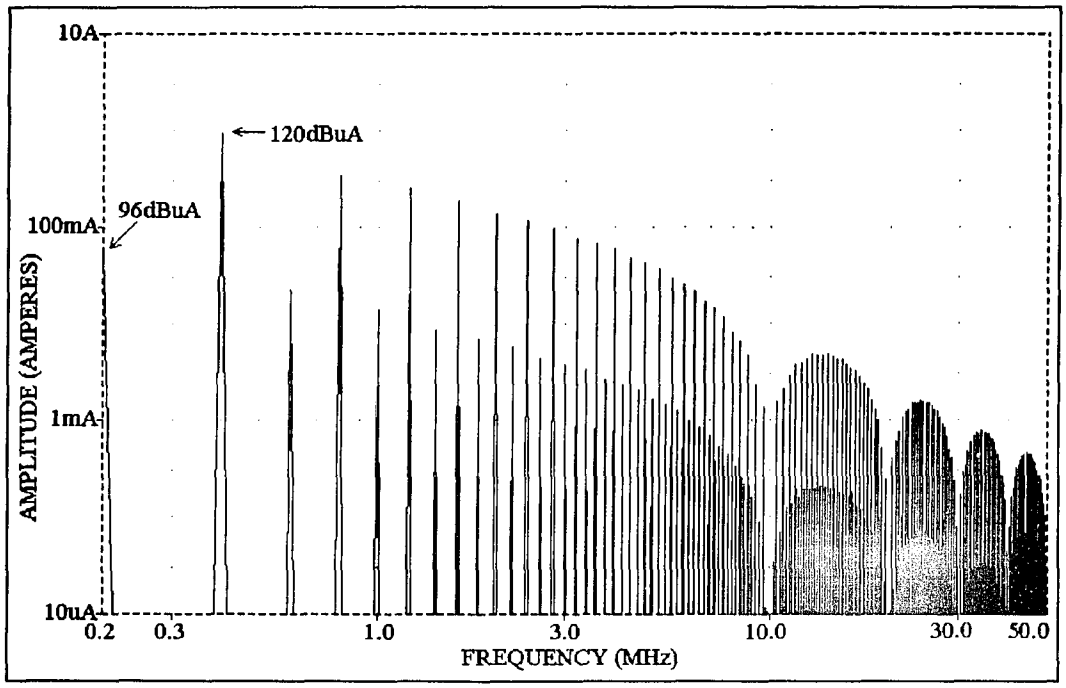

Figure 3.17-Simulated Input Current Waveforms Combined with a Phase Shift of 180°

In order to show that the filter can be successfully designed with a low frequency LC product one fourth the size of the original filter, the value of the low frequency inductor, L_L, is reduced by a factor of four. The original filter was modified to allow L_L to be removed and replaced with the smaller inductor. This eliminates the possibility of variations due to component tolerances or filter lay-out. The value of L_L is 44μH which is one fourth the value of the original 175μH inductor.

The original simulated filter was modified to incorporate the smaller inductor. The simulated current attenuation is shown in Figure 3.18. The attenuation at 200kHz is 79dB and 100dB at 400kHz. This filter should attenuate the waveform down to approximately 17dBμA at 200kHz and 20dBμA at 400kHz, well below the EMI limit. Figure 3.19 shows the simulated waveform after it has been filtered.

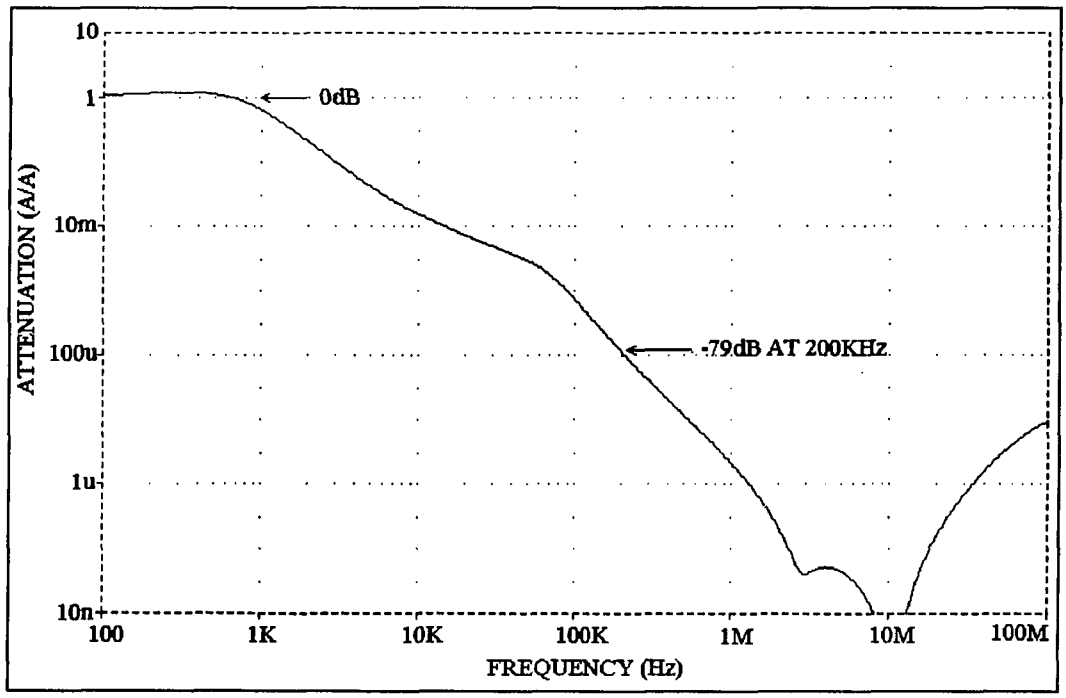

Figure 3.18-Attenuation of Simulated Filter for the Case Where the Two Waveforms are 180° Out of Phase

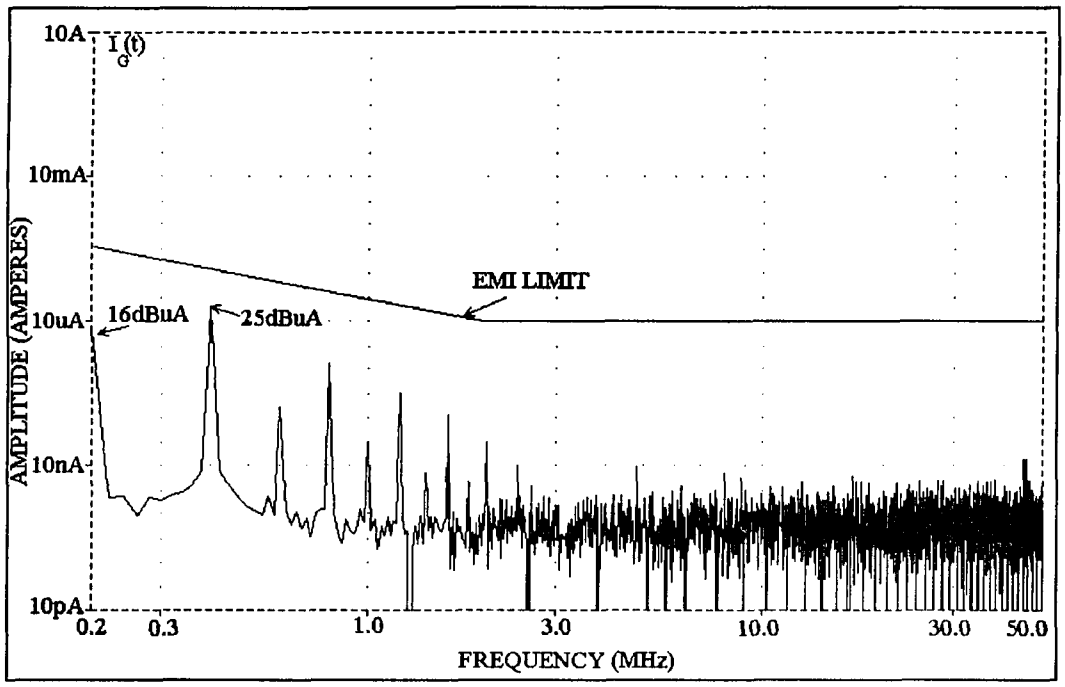

Figure 3.19-Simulated Filtered Output when Waveforms are Combined with 180° Phase Shift

Filter measurement:

The 175μH inductor in the original filter was removed and replaced with a 45μH inductor. With power applied to the voltage bus, the waveform was verified to be the two waveforms combined with 180° phase difference. The filtered output was then measured using the spectrum analyzer as shown in Figure 3.20. The harmonic magnitude at 200kHz is -81dBm and -78dBm at 400kHz. Once again, these values correspond very closely to those obtained by simulating the filtered waveforms. At 200kHz the simulated value was 16dBμA and the measured value converts to 17dBμA. At 400kHz the simulated value was 25dBμA and the measured value converts to 20dBμA.

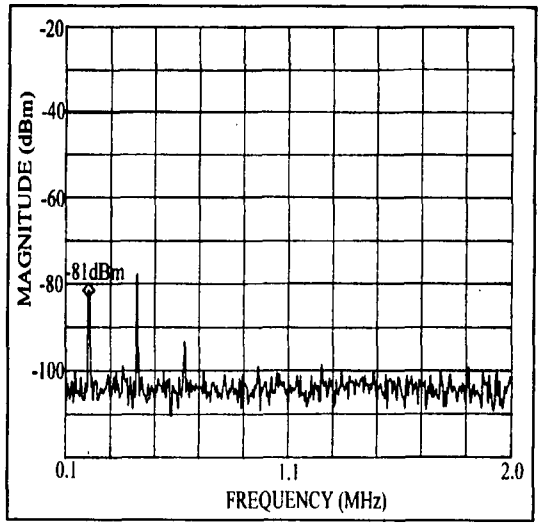

Figure 3.20-The Filtered Combined Input Current Waveform, $I_G(t)$, Shown in Figure 3.6.

CHAPTER 4

SUMMARY OF THESIS AND CONCLUSION

The Discontinuous Mode (DCM) Flyback Switched Mode Power Supply (SMPS) converts an input voltage into a desired output voltage through the use of a transformer, clamping diode, and a switching element. The switching element in this type of SMPS generates a triangular input current waveform that is conducted back onto the input voltage bus in the form of Electromagnetic Interference (EMI). This conducted EMI can exceed limits that are determined by the particular application of the SMPS. For example, a SMPS that is used in a military application may be required to meet MIL-STD-461 CE03, which is the military standard that states the maximum amount of EMI that can be conducted onto a power bus by a current waveform.

In Chapter 1, a typical DCM Flyback SMPS is simulated using the electronic circuit simulation tool, PSPICE, to demonstrate the amount of EMI that is conducted onto the input voltage bus by the input current generated by a single SMPS. The conducted EMI of the simulated SMPS is approximated by transforming the time varying input current waveform into the frequency domain by means of a Fourier Transform. The magnitude of each harmonic frequency is then scaled for direct comparison to MIL-STD-461 CE03 and is found to exceed the limit by 70 dB at the fundamental frequency. This simulated frequency spectrum is shown in Figure 1.7. In order for this SMPS to comply with MIL-STD-461 an EMI filter similar to the one shown in Figure 1.9 must be added to

the voltage bus. Since these filters are costly, both in the physical and monetary sense, it is important to minimize the amount of filtering that the EMI filter must provide.

In Chapter 2, the input current waveform of a typical DCM Flyback SMPS is modeled as an ideal triangular waveform. The low frequency accuracy of this model is demonstrated by a comparison of the frequency spectra of the input current waveform generated by a simulated DCM Flyback SMPS and an ideal triangular current waveform using PSPICE. The frequency spectrum of these waveforms are obtained by performing a Fourier Transformation on the individual time varying waveforms using PSPICE and are shown for comparison in Figure 2.3. The waveforms have identical harmonic magnitude for frequencies below about 10MHz. It is at this point that a resonance between the parasitic elements of the simulated SMPS occurs which causes the harmonic magnitude to increase above that associated with the ideal triangular waveform. For frequencies above this resonant point, the harmonic magnitude of the triangular waveform is actually larger than the simulated input current waveform. This is due to the fact that the sharp peaks of the ideal triangular waveform generate high frequency harmonics with greater magnitudes than the more rounded peaks of the simulated input current waveform. Since the EMI filter is designed to reduce the magnitude of the fundamental frequency, and by doing so provides sufficient attenuation for the higher frequency harmonics, this ideal triangular waveform is found to be an acceptable model for the input current waveform generated by a DCM Flyback SMPS.

When *n* SMPS share a common DC voltage input source, the individual input current waveforms combine on the input voltage bus. The manner in which these waveforms combine is determined by the switching frequency, phase relationships, duty cycles and peak amplitudes of the individual waveforms. It is these parameters that determine the amount of EMI that is conducted onto the input voltage bus by the combined input current waveforms.

In this work it is assumed that the system of multiple SMPS consists of DCM Flyback converters whose input current waveforms are represented by ideal triangular waveforms with identical switching frequencies and that the phase relationship between these waveforms can be controlled. It is the goal of this work to reduce the amount of combined EMI generated by this system by optimizing the phase relationship between the individual input current waveforms.

In order to predict the effect that the phase relationship has on the amount of EMI, *n* ideal triangular waveforms are combined with various phase shifts and the resultant EMI is examined. To do this in a systematic way, a symbolic Fourier Series representation is derived and shown in Equations 2.5-2.8, and is used to determine the optimum phase relationship that minimizes the EMI when the waveforms are combined. In the first part of the analysis discussed in Chapter 2.3 it is assumed that the waveforms are identical. In this case the largest amount of EMI occurs when the *n* waveforms combine with a phase shift of 0°. Here the frequency spectrum of the combined waveform retains the same fundamental frequency as the individual waveforms but the harmonic magnitude of the

combined waveform increases by a factor of n. An example of this is shown in Figure 2.9 where two identical waveforms with a switching frequency of 200KHz are combined with a phase shift of 0°. The fundamental frequency of this combined waveform is 200KHz and the resulting harmonics have twice the magnitude as the individual waveform. It is also shown that the amount of EMI is minimized when the same n waveforms combine with a phase shift equal to $360°/n$. Here n-1 out of n harmonics cancel and the fundamental frequency increased by a factor of n. An example of this is shown in Figure 2.11 where the frequency spectrum of the same two waveforms combined with a phase shift of 180° is given. Here it can be seen that 1 out of 2 harmonics have been canceled, the magnitude of the other harmonics remain the same as the previous case and the fundamental frequency increases to 400KHz.

When the effects that variations in amplitude and duty cycle have on the amount of combined EMI are examined in Chapter 2.6, it is shown that even though there is no longer a total cancellation of n-1 out of n harmonics, the magnitudes of these harmonics can be reduced enough to effectively increase the fundamental frequency of the combined waveform by a factor of n when the waveforms are combined with a phase shift equal to $360°/n$. An example of this is shown in Chapter 2.6.2 where the frequency spectrum of two waveforms that contain variations in amplitude and duty cycle are combined with phase shifts of 0° and 180°. In this case both waveforms have the same switching frequency of 200KHz but there is a 10% difference in both duty cycle and amplitude between the two waveforms. The frequency spectrum that results from combing these

two waveforms with a phase shift of 0° is shown in Figure 2.22. Here the fundamental frequency is 200KHz and the magnitude of the first and second harmonic is 806m and 305m Amperes respectively. When the same two waveforms are combined with a phase shift of 180° the resulting frequency spectrum of the combined waveform is shown in Figure 2.24. Here the magnitude of the odd harmonics are significantly less than the odd harmonics generated in the previous case. The magnitude of the first harmonic is down by 19dB. It is also worth noting that the magnitude of the even harmonics remains the same for both phase conditions.

Another advantage of combining n triangular waveforms with a phase shift equal to $360°/n$ is to reduce the amount of RMS current in the combined waveform. An example of this is shown in Chapter 2.7 where two identical waveforms are combined with a phase shift of 0° as shown in figure 2.8 and then 180° as shown in Figure 2.10. The RMS current for both cases is computed using Equation 2.22 and the RMS is compared. When the two waveforms are combined with a phase shift of 0° the RMS current is 0.82 Amperes (RMS). When the same two waveforms are combined with a phase shift of 180° the RMS current is 0.58 Amperes (RMS) which is 30% lower than the previous case.

This decrease in the amount of RMS current in the combined waveform reduces the power that is dissipated when the current flows through a resistive element. One type of resistive element that may be effected by the RMS current is the ESR associated with the low frequency shunt capacitor used in an EMI filter. If the ESR and the RMS current

are large, the capacitor must be able to dissipate the power without adversely effecting the operation of the capacitor.

To verify that the EMI in a system of n SMPS can be significantly reduced by combining the n input current waveforms with the optimal phase shift, a system of two DCM Flyback SMPS is designed and constructed and the results shown in the first part of Chapter Three. The input current waveforms generated by these two SMPS are designed to be identical but due to component differences there is a 0.2 Amperes variation between the peak amplitudes of the two waveforms. The system is designed to provide either a 0° or a 180° phase shift between the input current waveforms and the loads are fixed and identical. The combined EMI is then measured for both phase conditions. The two waveforms are first combined with a phase shift of 0° and the EMI is measured on the spectrum analyzer as shown in Figure 3.5. The phase shift is then changed to 180° and the EMI is again measured as shown in Figure 3.7. It is found by comparing these two figures that the magnitude of the even harmonics remains the same while the magnitude of the odd harmonics in the second case is significantly lower than in the first case. In fact the magnitude of the first harmonic is down by 22dB.

Even though the magnitude of EMI is substantially reduced by combining the waveforms with a phase shift of 180°, the conducted EMI in both cases exceeds the EMI limit described in MIL-STD-461 CE03. The harmonic magnitudes at the fundamental frequency are approximately 71dB and 49dB over the limit when the two waveforms are

combined with a phase shift of 0° and 180° respectively. In order to meet the above EMI requirement an EMI filter must be included.

The second part of Chapter Three contains the design, simulation, construction and experimental results of the EMI filters required for each case. It was shown in Chapter Two that if two identical waveforms with switching frequencies of 200KHz are combined with a phase shift of 180°, the fundamental frequency and all the other odd harmonics will cancel. This effectively moves the fundamental frequency from 200KHz to 400KHz and the LC product of the required EMI filter is reduced by a factor of four. This reduction can be seen from Equation 1.32 where the LC product refers to the low frequency capacitor and inductor that generate the low frequency roll-off point, F_O. When the fundamental frequency is doubled, F_O can be increased by the same amount and still provide sufficient attenuation at the fundamental frequency. By increasing F_O by a factor of two, the LC product is reduced by a factor of four.

Even though the two waveforms in this system are not identical, it is shown that the LC product of the EMI filter can be reduced by a factor of four if the two waveforms are combined with a phase shift of 180°. To show this an EMI filter is first designed for the 'worst' case where the two waveforms are combined with a phase shift of 0°. The value of the low frequency inductor is then reduced by a factor of four and used to filter the combined current when the phase shift is changed to 180°. To show this, the 'worst' case EMI filter is designed and simulated. The design of this filter is shown in Figure 3.11 with the parasitic elements included. The parasitic elements were measured and included

in the PSPICE simulation to determine the effect they have on the attenuation of the filter. Figure 3.12 shows the attenuation with the corner frequencies defined in terms of filter components and parasitic elements. In order to simulate the ability of this filter to properly attenuate the combined waveform, the input current waveforms that were generated by the two SMPS are also simulated on PSPICE where they are combined with a phase shift of 0° and transformed into the frequency domain by a Fourier transform as shown in Figure 3.8. A comparison of the simulated and measured frequency spectrum of the combined current waveforms show that the simulated waveforms generate a frequency spectrum that is within 2dB of the measured frequency spectrum shown in Figure 3.5. The simulated combined waveform is then filtered by the simulated filter and the filtered output is shown in Figure 3.15. This simulation shows that an attenuation of 91dB can be expected at the fundamental frequency by this filter.

The filter is then constructed and used to filter the combined input current waveform generated by the two SMPS. The filtered waveform is shown in Figure 3.16 were it can be seen that the filter attenuation at the fundamental frequency is 98dB which is very close to the simulated filter attenuation of 91 dB.

The low frequency inductor is then reduced by a factor of four and the input current waveforms are combined with a phase shift of 180°. A simulation is performed with the modeled waveforms combined with a phase shift of 180° and the low frequency inductor reduced in value by one fourth. The simulated attenuation of this filter is shown in Figure 3.18 where the attenuation at the switching frequency is given as 79dB. The

filtered combined waveform is then measured on the spectrum analyzer and the attenuation at the switching frequency is 81dB which is very close to the simulated attenuation of 79dB. In both cases the filtered waveforms are well below the EMI limit specified by MIL-STD-461 CE03. The amount of inductance needed for the case when the two waveforms are combined with a phase shift of 180° is 25% less than needed when the waveforms are combined with a phase shift of 0°.

REFERENCES

[1] A. Wang and S. Sanders, "Programmed Pulsewidth Modulated Waveforms for Electromagnetic Interference Mitigation in DC-DC Converters," IEEE Transactions Power Electronics, Vol. 8, No. 4, October 1993, pp. 596-604.

[2] M. Nave, "Measuring, suppressing and Filtering Common Mode Emissions in Switched Mode Power Supplies," Technical Papers of the Fourth International High Frequency Power Conversion 1989 Conference, 1989, pp. 285-293.

[3] T. Guo, "Diagnosis of Power Supply Conducted EMI Using a Noise Separator," APEC '95. Tenth Annual Applied Power Electronics Conference and Exposition, Conference Proceedings 1995, Vol. 1, pp. 259-266.

[4] R. D. Middlebrook, "Design Techniques for Preventing Input Filter Oscillations in Switched-Mode Regulators," Proceedings of the Fifth National Solid-State Power Conversion Conference, Powercon 5, May 1978, pp. A3-1 through A3-16.

[5] H. Zong-Yu, "Analysis and Design of EMI Filter for Multi-Output Switching Mode Power Supply," Intelec. Sixteenth International Telecommunications Energy Conference, 1994 Record, pp. 457-463.

[6] L. Hsiu, M. Goldman, R. Carlsten, A. Witulski, and W. Kerwin, "Characterization and Comparison of Noise Generation for Quasi-Resonant and Pulsewidth-Modulated Converters," IEEE Transactions on Power Electronics, Vol. 9, No. 4, July 1994, pp. 425-432.

[7] R. W. Erickson, Power Electronics I, Course notes for ECE 561, University of Arizona Department of Electrical and Computer Engineering, Copyright © 1984 by R. W. Erickson.

[8] M. Nave, Power Line Filter Design for Switched-Mode Power Supplies, Copyright © 1991 by Van Nostrand Reinhold.

[9] J. Kassakian, M. Schlecht and G. Verghese, Principles of Power Electronics, Copyright © 1991 by Addison-Wesley Publishing Company, Inc.

[10] M. Nave, "EMI: An Introductory Tutorial," Technical Publications, EMC Services, Inc., Vol. II.

[11] M. Nave, "MIL-STD-461: CE01 vs. CE03," Technical Publications, EMC Services, Inc., Vol. I.

REFERENCES (*Continued*)

[12] F. Zollner, "EMI Considerations for High Frequency Power Supplies," Technical Papers of the Seventh International High Frequency Power Conversion 1992 Conference, 1992 Record, pp. 103-111.

[13] F. Stremler, Introduction to Communications Systems, Copyright © 1982 by Addison-Wesley Publishing Company, Inc.

[14] E. Kreyzig, Advanced Engineering Mathematics, Copyright © 1988 by John Wiley & Sons, INC.